NeuroImage 52 (2010) 1041–1058

Contents lists available at ScienceDirect

NeuroImage

journal homepage: www.elsevier.com/locate/ynimg

Bifurcation analysis of neural mass models: Impact of extrinsic inputs and dendritic time constants

Andreas Spiegler [a,b,*], Stefan J. Kiebel [a], Fatihcan M. Atay [c], Thomas R. Knösche [a]

[a] Max Planck Institute for Human Cognitive and Brain Sciences, Leipzig, Germany
[b] Institute of Biomedical Engineering and Informatics, Technical University Ilmenau, Germany
[c] Max Planck Institute for Mathematics in the Sciences, Leipzig, Germany

ARTICLE INFO

Article history:
Received 2 September 2009
Revised 17 December 2009
Accepted 21 December 2009
Available online 4 January 2010

ABSTRACT

Neural mass models (NMMs) explain dynamics of neuronal populations and were designed to strike a balance between mathematical simplicity and biological plausibility. They are currently widely used as generative models for noninvasive electrophysiological brain measurements; that is, magneto- and electroencephalography (M/EEG). Here, we systematically describe the oscillatory regimes which a NMM of a single cortical source with extrinsic input from other cortical and subcortical areas to each subpopulation can explain. For this purpose, we used bifurcation analysis to describe qualitative changes in system behavior in response to quantitative input changes. This approach allowed us to describe sequences of oscillatory regimes, given some specific input trajectory. We systematically classified these sequential phenomena and mapped them into parameter space. Our analysis suggests a principled scheme of how complex M/EEG phenomena can be modeled parsimoniously on two time scales: While the system displays fast oscillations, it slowly traverses phase space to another qualitatively different oscillatory regime, depending on the input dynamics. The resulting scheme is useful for applications where one needs to model an ordered sequence of switching between qualitatively different oscillatory regimes, for example, in pharmacological interventions, epilepsy, sleep, or context-induced state changes.

Introduction

Dynamic brain signals like magneto- and electroencephalography (M/EEG) contain a wealth of information on brain function. To access this information and describe the associated cognitive processes, these measurements are usually acquired under defined conditions (e.g., stimulation patterns and behavior, sleep stage, general vigilance, pathologies). For statistical analysis, one can use *generative models* that describe the mapping from the generating states to the observed data. It is particularly useful if these models are *biologically plausible*, in the sense that the state variables and parameters are anatomically and/or biophysically meaningful. This provides the opportunity to map the measurements to physically meaningful quantities by inverting (i.e., fitting) the model and to test mechanistic hypotheses concerning the underlying brain function. To ensure that the inversion is mathematically tractable and at the same time physically meaningful, the model must strike a balance between mathematical simplicity and biological realism.

In contrast to single neuron models such as simple integrate-and-fire models (Abbott, 1999) and the more elaborate Hodgkin and Huxley type of models (FitzHugh, 1955; Hindmarsh and Rose, 1984; Hodgkin and Huxley, 1952; Nagumo et al., 1962), neural mass models (Freeman, 1978; Jansen and Rit, 1995; Jansen et al., 1993; Lopes da Silva et al., 1974, 1976; Nunez, 1974) describe brain function at a mesoscopic scale. These models quantify the mean firing rates and mean membrane potentials of large neuronal populations, so-called *neural masses* (NM), using differential equations. The approach provides a parsimonious yet biophysically meaningful description of M/EEG phenomena.

In this work, we deal with a specific but widely used choice of neural mass model (NMM) first described by Jansen and Rit (Jansen and Rit, 1995; Jansen et al., 1993), which is based on previous modeling work by Lopes da Silva et al. (1974, 1976). The Jansen and Rit model of a cortical area (or column) consists of three interconnected NMs (pyramidal cells, excitatory and inhibitory interneurons). It has been used to explain both epilepsy-like brain activity (Wendling et al., 2002, 2000) and various narrow band oscillations ranging from the delta to the gamma frequency bands (David and Friston, 2003). A natural extension of this approach is to model a network of cortical areas as a collection of coupled single-area Jansen and Rit models (David and Friston, 2003; David et al., 2005;

* Corresponding author.
E-mail address: spiegler@cbs.mpg.de (A. Spiegler).

1053-8119/$ – see front matter © 2010 Elsevier Inc. All rights reserved.
doi:10.1016/j.neuroimage.2009.12.081

David et al., 2006; Jansen and Rit, 1995; Sotero et al., 2007; Wendling et al., 2000), thereby accounting for more complex transient and oscillatory behavior. The Bayesian inversion of these dynamic generative models given M/EEG data (referred to as 'Dynamic Causal Modeling' (DCM) (David et al., 2006; Kiebel et al., 2009a)) has been developed for the analysis of event-related (David et al., 2006; Kiebel et al., 2006, 2007) and steady-state responses (Moran et al., 2009). These techniques, using the Jansen and Rit model, have been used experimentally to test novel hypotheses about brain function at a systems level (Garrido et al., 2007, 2009; Schofield et al., 2009) and are available in the widely distributed free academic software 'Statistical Parametric Mapping' (Friston et al., 2007).

In this paper, we analyze the neural mass model used in DCM, which includes the original Jansen and Rit model as a special case: In the 'extended Jansen and Rit model', extrinsic input may target the two populations of interneurons (David et al., 2005). Here, we focus on the single-area version of this extended Jansen and Rit model and ask the question which dynamic regimes this single-area model can experience. To do this, we investigate the entire effective parameter space of the model, rather than just the specific parameter set proposed by Jansen and Rit (1995). As we will show, our analysis produces a catalogue of dynamic regimes, which can be directly used for modeling M/EEG data. We found that the dynamics of the single-area model are richer and probably more useful for modeling purposes than previously thought. This means that one can model a large class of phenomena with the single-area extended Jansen and Rit model. Comprehensive knowledge about single-area dynamics, as provided by our results, may therefore be valuable for the network analysis of M/EEG and electrophysiology data using Bayesian model inversion schemes like DCM.

We systematically describe the dynamic properties of the extended Jansen and Rit model as a function of its key parameters. There are rich dynamics expressed by bifurcations (i.e., sudden transitions in dynamic behavior) and limit cycle (LC) branches which have not been described before (Grimbert and Faugeras, 2006). We use *bifurcation diagrams*, which are compact and intuitively accessible representations of the behavior of dynamic systems plotted against changing parameters. Knowledge of this dynamic behavior is an important tool because it tells the modeler how the system will behave qualitatively when system parameters change slowly. We systematically classify LC branches and discuss the associated dynamics in detail, including their conditions of changing as a function of key parameters, namely the extrinsic inputs from other cortical and subcortical areas to the three NMs and the dendritic time constants. This bifurcation analysis yields a comprehensive catalogue of potential oscillatory regimes. A potential use of this catalogue is that the modeler can decide whether the single-area extended Jansen and Rit NMM is sufficient to model any specific phenomenon (e.g., M/EEG) or whether a more complex model, such as a network of areas, should be chosen. Moreover, the modeler can use the catalogue to select a specific parameter set that best reproduces the observed signals.

In addition, the bifurcation diagrams inform the modeler which slow-moving trajectories through parameter space will cross bifurcation points. This means that apparently complex M/EEG phenomena can be explicitly modeled as an ordered sequence of switches between different oscillatory regimes. In principle, this enables one to model phenomena like the progression of pathology, epileptic events (see, e.g., Marten et al., 2009; Rodrigues et al., 2009; Suffczynski et al., 2005, for thalamocortical models), pharmacological intervention, sleep stages (Steyn-Ross et al., 2005), or general changes in the oscillatory regime due to contextual state changes. We illustrate this approach using some synthetic examples. Our analysis in this paper enables the selection of a highly constrained parameterization. Bayesian inversion (as used in DCM) should, in principle, be able to identify the free parameters of ordered sequence models, for example, the slowly changing function needed to induce the switching behavior.

To our knowledge, our paper is the first to classify principal types of system topology of the single-area extended Jansen and Rit model. In particular, we will show that the parameterization chosen by Jansen and Rit (1995) gives rise to quite specific system behavior which is an expectation rather than the rule among the different dynamic regimes. More generally, we will show that the predominant asymptotic behaviors over the entire parameter space are harmonic oscillations of a LC branch, arising from two Andronov–Hopf bifurcations with oscillation frequency between 0 and 80 Hz.

The remainder of the paper is organized as follows. In the Materials and methods section, we first describe the extended NMM for a single cortical area and the bifurcation analysis. The Results section describes and discusses the precise set-up and the outcomes of the analyses, both at a general level and by means of specific examples. Finally, the Discussion section provides a more general appraisal of the results, thereby pointing out the usefulness for both specific modeling scenarios and more general considerations.

Materials and methods

To make the methodology and consequently our results and conclusions accessible to the broad readership of NeuroImage, we have chosen a 'verbose' style of presenting technical details. We will first introduce a NMM of a cortical area. Then, we will derive the parameter space for our analysis of the dynamic properties of that model. Finally, we will provide a brief introduction to system analysis using bifurcation diagrams and describe how we use this technique to characterize the dynamics of the extended Jansen and Rit neural mass model.

The neural mass model of a cortical area

The neural mass model (NMM) of Jansen and Rit (Jansen and Rit, 1995; Jansen et al., 1993) describes a small local network representing a *cortical area*. This basic circuit, consisting of pyramidal cells (PCs) with feedback loops mediated by excitatory and inhibitory interneurons (EINs and IINs), has been described in a number of studies (e.g., David and Friston, 2003; Jansen and Rit, 1995; Jansen et al., 1993; Lopes da Silva et al., 1976; Spruston, 2008; Wendling et al., 2002; Wendling et al., 2000). Here, after a brief review of the underlying firing rate approach, we will formulate a cortical area model which is an extension of the original Jansen and Rit NMM.

Neural mass–firing rate model

The state space of the dynamic *firing rate model* (e.g., Gerstner and Kistler, 2002; Wilson and Cowan, 1972) comprises the mean firing rate and the mean membrane potential of a local population of similar neurons (typically some tens of thousands), referred to as neural mass (NM). Two conversion operators are used: a linear rate-to-potential operator that captures the mean synaptic response function and an instantaneous nonlinear potential-to-rate operator, accounting for the mean firing pattern as a function of the mean membrane potential.

The *rate-to-potential operator* computes the mean postsynaptic potential (PSP) at the soma for a target neuron b (relative to the resting potential) by convolution of a synaptic kernel $h_{ba}(t)$ with the mean firing rate m_a of neuron a:

$$v_{ba}(t) = c_{ba} \cdot (h_{ba} \otimes m_a)(t). \tag{1}$$

The constant c_{ba} is proportional to the average number of synaptic contacts established between the two NMs a and b. The kernel first proposed by Rall (Jack et al., 1975; Rall, 1964, 1967) can be interpreted as the PSP elicited by a single incoming spike. It has been found to adequately describe the synaptic spike response

(Freeman, 1975; Jack et al., 1975; see also Jansen et al., 1993, and the references cited therein).

$$h_{ba}(t) = \begin{cases} H_{ba}\frac{t}{\tau_{ba}}e^{-\frac{t}{\tau_{ba}}} & t \geq 0 \\ 0 & t < 0 \end{cases}. \quad (2)$$

It is parameterized by the average synaptic gain H_{ba} and the average dendritic time constant τ_{ba}. Both are grouped representations for all cells belonging to the NM and characterize the synaptic–dendritic transmission processes. The synaptic gains represent the maximum magnitude of the PSPs. The dendritic time constants τ_{ba} constitute a combined representation of passive dendritic cable delays and neurotransmitter kinetics, predominantly corresponding to fast synaptic activity (AMPA and $GABA_A$) (Liley et al., 2002). This approach relies on some simplifying assumptions (Ermentrout, 1998). The first assumption is that the width of the spikes is negligible (e.g., it can be modeled as a Dirac's delta function). The second assumption is that the effects of different spikes add up linearly (summators in Fig. 1), which ignores any reciprocal influences between synapses and active dendritic behavior.

The kernel function (2) can be interpreted as Green's function of a second-order ordinary differential equation, which can be expressed as two first-order linear inhomogeneous differential equations:

$$\begin{aligned} \dot{v}_{ba} &= u_{ba} \\ \dot{u}_{ba} &= \frac{H_{ba}}{\tau_{ba}} m_a(t) - \frac{2}{\tau_{ba}} u_{ba} - \frac{1}{\tau_{ba}^2} v_{ba}. \end{aligned} \quad (3)$$

The *potential-to-rate operator* transfers the mean PSP (i.e., $v_b = \sum_a v_{ba}$, the membrane potential at the axonal hillock) to the mean firing rate by means of a sigmoid function. The sigmoid can be interpreted as an approximation of the superposition of many Heaviside (step) functions with Gaussian-distributed threshold values (Marreiros et al., 2008; Wilson and Cowan, 1972). It is specified by firing threshold v_{b0}, maximum mean firing rate $2 \cdot e_{b0}$, and slope at the firing threshold r_b

$$m_b(t) = S_b(v_b) = \frac{2 \cdot e_{b0}}{1 + e^{r_b(v_{b0} - v_b(t))}}. \quad (4)$$

The firing threshold v_{b0} can be interpreted as excitability of the NM. At this point, half of the maximum firing rate e_{b0} is reached with the maximal slope $e_{b0} \cdot r_b / 2$. The slope r_b reflects the variance of the firing thresholds within the NM. For a more detailed and rigorous treatment of the potential-to-rate operator of a NM, see Liley et al. (2002).

Model for a cortical area

Although local neuronal circuits are complex (see, e.g., Thomson and Bannister, 2003), there is a strong tendency for local axonal collaterals of PCs in cortical layers III to VI to make synaptic contacts to GABAergic interneurons, which themselves have only short axonal processes and therefore contact local cells, such as PCs. This forms intralaminar (PCs in layers III to VI) as well as interlaminar (PCs in layers III and IV) inhibitory feedback loops. Feedback loops may also be excitatory (glutamatergic), mediated either by (smaller) PCs or by EINs, mostly so-called spiny stellate cells in layer IV (Markram et al., 2004; Thomson and Bannister, 2003). Therefore, the membrane potential of the PCs can be modeled as a weighted sum of the effects of extrinsic inputs to the cortical areas and feedback influences from interneurons.

When reducing the local neuronal circuitry to a parsimonious model, the following points seem to be important: (1) there are PCs sending axons to other brain areas which, due to their long apical

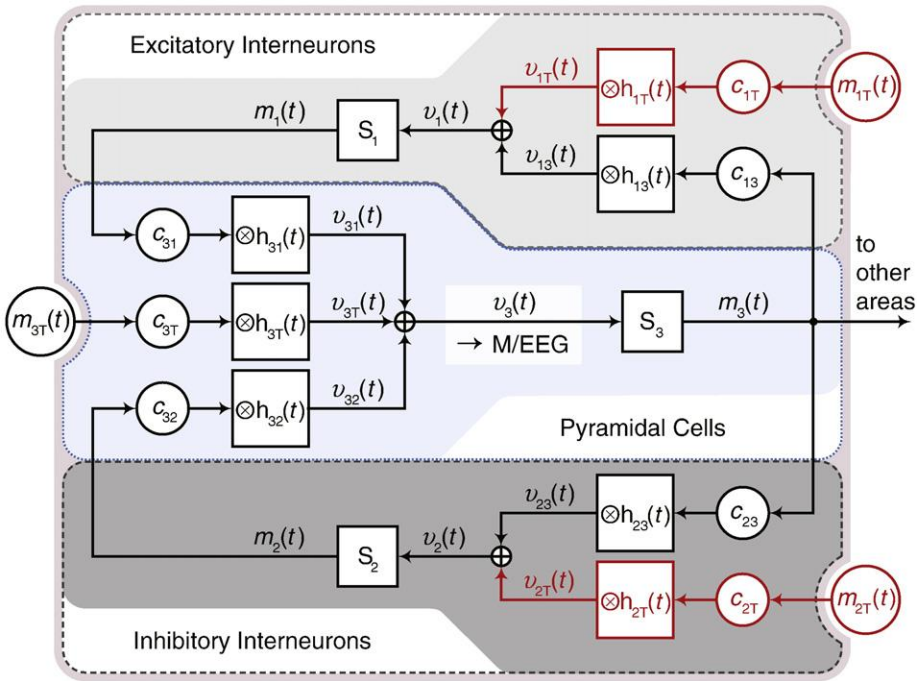

Fig. 1. Extended structure of the model for a cortical area. The model consists of three neural masses, representing pyramidal cells receiving positive and negative feedback via EINs or IINs. Operators (boxes) are S – the potential-to-rate operator transforming the mean membrane potential to the average firing rate at the axon hillock, $\otimes h_{ba}(t)$ – the rate-to-potential operator computing the mean postsynaptic potential at the soma for a neural mass b by convolution of the synaptic kernel $h_{ba}(t)$ (including the dendritic time constants) with the incoming mean firing rate m_a of neuron a weighted according to the mean number of synaptic contacts c_{ba}, and $\oplus$ – the summation operator gathering the postsynaptic potentials rising in the dendritic tree at the soma. Parameters (circles) are c_{ba} – the average number of synaptic contacts established between neural mass a to b and $m_{bT}(t)$ – the extrinsic input firing rate of the neural mass b, with a, b assuming 1 (EINs), 2 (IINs), 3 (PCs), and T (extrinsic input). The system variables (describing the flows) are $m_b(t)$ – the mean firing rate of the neural mass b, and $v_{ba}(t)$ – the membrane potential of neural mass b due to input a. Mean postsynaptic potentials of pyramidal cells $v_3(t)$ mainly contribute to M/EEG. Extensions to the classical structure of Jansen and Rit (1995) are drawn in red.

dendrites arranged in parallel, give rise to measurable EEG and MEG (Lopes da Silva and van Rotterdam, 1999b), (2) collaterals from these PCs contact excitatory and inhibitory cells with local axonal arbors (interneurons), and (3) these interneurons have a high probability to in turn, make synaptic contacts with the PCs, thus forming feedback loops. In line with this, Jansen and Rit (1995) described the cortical area[1] as a basic element composed of three NMs: PCs, EINs and IINs, interacting through positive and negative feedback loops. In their model, extrinsic input (i.e., from other brain areas) only targets the PCs. However, since there is strong evidence that this input also targets interneurons, the model was extended accordingly (David et al., 2005). Its structure is illustrated in Fig. 1.

Note that the feedback loops may be modeled dynamically (see, e.g., Breakspear and Jirsa, 2007; Jirsa and Haken, 1996; Nunez, 1974; Robinson et al., 2002) (when also considering propagation delays, see, e.g., Marten et al., 2009; Rodrigues et al., 2009). However, in our model, the connections are assumed to be local (within a single area). That means we assume only small spatial extension and transmission times, and therefore describe the feedback connection by a gain constant.

The mean membrane potential of the PCs is caused by three different inputs: excitatory input from local EINs, excitatory input from other areas (referred to as extrinsic inputs), and inhibitory input from local IINs, $v_3(t)=v_{31}(t)+v_{3T}(t)+v_{32}(t)$. The output of the PCs is fed back into the EINs and IINs, thus closing the feedback loops. In contrast to the original paper by Jansen and Rit (1995), the present NMM takes into account extrinsic input from other cortical and/or subcortical areas not only to the PCs ($m_{3T}(t)$), but also to both types of interneurons ($m_{1T}(t)$ and $m_{2T}(t)$). This approach, first used by David, Harrison and Friston (2005), is based on findings that interneurons also receive input from other cortical areas. For example, the spiny stellate cells (EINs) as well as GABAergic basket cells (IINs) in layer IV of primary sensory cortices receive input from the thalamus (e.g., Ahmed et al., 1997; Staiger et al., 2004; Stratford et al., 1996). This is also in line with inter-area connection schemes as postulated, for example, by Felleman and Van Essen (1991).[2] The neuronal currents underlying M/EEG generation are believed to be produced mainly by the membrane potentials of the PCs (Lopes da Silva and van Rotterdam, 1999a) as a result of the asymmetric shape of these cells (with apical dendrites) and their parallel alignment perpendicular to the cortical surface (Braitenberg and Schüz, 1991). The linear output function (leadfield), mapping the mean membrane potentials of the PCs to the measurements outside the brain, has to take into account a physical model of the head (Kiebel et al., 2006). In this work, it is not necessary to consider leadfield modeling because we model only a single area.

The extended NMM of a cortical area, as sketched in Fig. 1, can be described by the following system of 14 nonlinear first-order differential equations.

Pyramidal cells to excitatory interneurons (3 → 1)

$$\begin{aligned}\dot{v}_{13} &= u_{13}\\ \dot{u}_{13} &= \frac{H_{13}}{\tau_{13}}c_{13}S_3(v_{31}+v_{32}+v_{3T})-\frac{2}{\tau_{13}}u_{13}-\frac{1}{\tau_{13}^2}v_{13}\end{aligned} \tag{5}$$

Pyramidal cells to inhibitory interneurons (3 → 2)

$$\begin{aligned}\dot{v}_{23} &= u_{23}\\ \dot{u}_{23} &= \frac{H_{23}}{\tau_{23}}c_{23}S_3(v_{31}+v_{32}+v_{3T})-\frac{2}{\tau_{23}}u_{23}-\frac{1}{\tau_{23}^2}v_{23}\end{aligned} \tag{6}$$

Excitatory interneurons to pyramidal cells (1 → 3)

$$\begin{aligned}\dot{v}_{31} &= u_{31}\\ \dot{u}_{31} &= \frac{H_{31}}{\tau_{31}}c_{31}S_1(v_{13}+v_{1T})-\frac{2}{\tau_{31}}u_{31}-\frac{1}{\tau_{31}^2}v_{31}\end{aligned} \tag{7}$$

Inhibitory interneurons to pyramidal cells (2 → 3)

$$\begin{aligned}\dot{v}_{32} &= u_{32}\\ \dot{u}_{32} &= \frac{H_{32}}{\tau_{32}}c_{32}S_2(v_{32}+v_{2T})-\frac{2}{\tau_{32}}u_{32}-\frac{1}{\tau_{32}^2}v_{32}\end{aligned} \tag{8}$$

Extrinsic input to excitatory interneurons (T → 1)

$$\begin{aligned}\dot{v}_{1T} &= u_{1T}\\ \dot{u}_{1T} &= \frac{H_{1T}}{\tau_{1T}}c_{1T}m_{1T}(t)-\frac{2}{\tau_{1T}}u_{1T}-\frac{1}{\tau_{1T}^2}v_{1T}\end{aligned} \tag{9}$$

Extrinsic input to inhibitory interneurons (T → 2)

$$\begin{aligned}\dot{v}_{2T} &= u_{2T}\\ \dot{u}_{2T} &= \frac{H_{2T}}{\tau_{2T}}c_{2T}m_{2T}(t)-\frac{2}{\tau_{2T}}u_{2T}-\frac{1}{\tau_{2T}^2}v_{2T}\end{aligned} \tag{10}$$

Extrinsic input to pyramidal cells (T → 3)

$$\begin{aligned}\dot{v}_{3T} &= u_{3T}\\ \dot{u}_{3T} &= \frac{H_{3T}}{\tau_{3T}}c_{3T}m_{3T}(t)-\frac{2}{\tau_{3T}}u_{3T}-\frac{1}{\tau_{3T}^2}v_{3T}\end{aligned} \tag{11}$$

The extrinsic inputs from other cortical and subcortical areas are modeled by noisy processes, here denoted by $m_{1T}(t)$, $m_{2T}(t)$ and $m_{3T}(t)$ for the extrinsic afferents T on NM 1 for EINs, NM 2 for IINs and NM 3 for PCs.

Parameter space

Dimension reduction

In this work, we explore the dynamics of the single-area model as a function of the five system parameters which are most relevant for the richness of the dynamics: the dendritic time constants (excitatory and inhibitory) and the extrinsic input (i.e., from other cortical and subcortical areas) to the three NMs. In the following, we will justify this choice.

In the form described in Eqs. (5) to (11), the system has 33 parameters,[3] which renders any exhaustive analysis prohibitive. Following the suggestions of Jansen and Rit (1995), the rate-to-potential operators were only distinguished between excitatory and inhibitory synaptic contacts, described by the kernels $h_e(t)$ and $h_i(t)$. The afferent connections originating from the PCs and EINs are exclusively excitatory (i.e., $h_{13}(t)=h_{23}(t)=h_{31}(t)=h_e(t)$). Afferents from IINs are inhibitory (i.e., $h_{32}(t)=h_i(t)$). Extrinsic afferents (i.e., from other cortical or subcortical areas) could be excitatory or inhibitory (i.e., $h_{bT}(t)=\{h_e(t),\ h_i(t)\}$, $b=\{1,\ 2,\ 3\}$). Moreover, we assume that the products of average synaptic gains and dendritic time

[1] Jansen and Rit (1995) identified this network with a *cortical column* according to the findings of Mountcastle (1957). However, because the universality of the concept of columnar organization of the cortex is controversial (Horton and Adams, 2005), we use the term *cortical area* instead. The key mechanisms of the model are unaffected by this reinterpretation.

[2] The extended model as analyzed here can be related to the original model of Jansen and Rit (1995) without extrinsic inputs to the interneurons as follows. Variation in the extrinsic input levels in the extended model is equivalent to variation in the firing thresholds of the corresponding target NMs in the original model if, and only if, the extrinsic inputs are constant in time (or change slowly as compared to the time constants of the system).

[3] These are the following: the intrinsic dendritic time constants τ_{ba}, synaptic gains H_{ba} and contact numbers c_{ba} with ba = {13, 23, 31, 32}; the parameters of the three sigmoid functions (3 parameters each) S_b; the extrinsic input levels to the three neural masses m_{bT}; the extrinsic dendritic time constants τ_{bT}, synaptic gain H_{bT}, and contact numbers c_{bT} with b = {1, 2, 3}.

Table 1
Effective ranges of the extrinsic input of the extended model for a cortical area. Positive and negative postsynaptic potentials are due to excitatory and inhibitory inputs.

Extrinsic input on	Postsynaptic potentials (mV)		Maximum firing rate (s^{-1})	
	Min	Max	Excitatory input	Inhibitory input
Excitatory interneurons	−26.63	16.69	513.54	60.52
Inhibitory interneurons	−10.18	16.69	513.54	23.12
Pyramidal cells	−22.24	90.94	2798.16	50.55

Table 2
Range of the varied system parameters: dendritic time constants for inhibitory and excitatory synaptic terminals $\tau_{e,i}$ and postsynaptic potentials due to extrinsic afferent projections on excitatory v_{1T} inhibitory interneurons v_{2T} and pyramidal cells v_{3T}.

Parameter	Range	Step size	Unit
$\tau_{e,i}$	[2,60]	2	ms
v_{1T}	{−27, −22, −17, −12, −8, −4, −2, 0, 2, 4, 8, 12, 17}	Discrete	mV
v_{2T}	{−11, −8, −4, −2, 0, 2, 4, 8, 12, 17}	Discrete	mV
v_{3T}	[−22.24, 90.94]	Continuous	mV

constants are constant, $H_{e,i} \cdot \tau_{e,i} = \varepsilon_{e,i}$, which is supported by computational modeling (Agmon-Snir and Segev, 1993; Williams and Stuart, 2003). The respective constant products for both cases $\varepsilon_e = 32.5$ μV s and $\varepsilon_i = 440$ μV s are derived from the Jansen and Rit configuration, similar to the definition used by David and Friston (2003). As shown later, these constraints fix the equilibrium states of the system under the condition of constant extrinsic inputs to INs. The synaptic contact numbers for the extrinsic inputs just linearly scale the extrinsic inputs and can therefore be fixed to unity in our analysis (i.e., $c_{bT} = 1, b = \{1, 2, 3\}$). Finally, following Jansen and Rit (1995), the parameters of the sigmoid function were assumed to be the same for all NMs.

Of the remaining 18 free parameters, the dendritic time constants (τ_e and τ_i) and the extrinsic inputs levels ($m_{1T}(t)$, $m_{2T}(t)$, and $m_{3T}(t)$) were selected for further analysis. The time constants were chosen because they were expected to exercise a major influence on the system's ability to oscillate and the frequency of these oscillations. The constant (or slowly changing, relative to the time constants of the system) extrinsic input levels to the three NMs are of major importance if the system is part of a larger network of cortical areas. They depend upon extrinsic connections (between areas), which have been used to account for experimental observations in DCM (David et al., 2005).

Here, we did not analyze the parameters of the sigmoid (Eq. (4)), and the intrinsic synaptic contact numbers. Variations in the extrinsic input levels, which we do analyze, are equivalent to variation in firing thresholds of the sigmoid functions and to variations in intrinsic synaptic contact numbers (c_{13}, c_{23}, c_{31}, c_{32}) if the system has a stable fixed point, and the extrinsic inputs change slowly relative to the time constants of the system. Therefore, these parameters were not varied, but chosen according to the suggestions of Jansen and Rit (1995).

To summarize, we capture the dynamics of the system by varying five parameters: the extrinsic input levels to the three NMs, and the excitatory and inhibitory dendritic time constants. The reduction to five effective control parameters implies stable manifolds in the original 14-dimensional state space, thus allowing its reduction to 12 dimensions.[4]

It should be pointed out that this type of analysis can be modified or extended in several ways, for example, by using other system parameters for the bifurcation analysis, by using higher codomains, or by applying the analysis to other models, for example, networks of several single-area NMMs.

Effective range of parameters

To ensure that the analysis is complete with respect to the five-dimensional parameter space chosen, we determined the effective ranges of the analyzed parameters (see Tables 1 and 2). The nonlinear properties of the potential-to-rate operator greatly reduce the effective ranges of extrinsic inputs in a biophysically plausible fashion.

By definition, the PSP of any NM can reach arbitrary values due to the unconstrained extrinsic input firing rates. However, the saturation property of the potential-to-rate operator (sigmoid function) limits the impact of such PSP changes on the mean firing rate of the NM. Due to its sigmoidal shape, the potential-to-rate operator has a limited effective dynamic range $[v_0 - v_S,\ v_0 - v_S]$. We use the following definition for v_S. According to Eq. (4), the maximum slope of the sigmoid function, and hence the maximum influence of the PSP changes on the output firing rate, occurs around the firing threshold v_0 with

$$s_{max} = \frac{\partial}{\partial v} S(v_b)\big|_{v_b = v_{b0}} = \frac{e_{b0} r_b}{2}. \tag{12}$$

The effective range (around the firing threshold v_{b0}) is taken to be the PSP value for which the slope of the function has dropped to $\alpha \cdot s_{max}$. For example, $\alpha = 0.01$ yields $v_S = r_b^{-1} \cdot \log(199 + 60 \cdot 11^{1/2})$. For standard parameters (Jansen and Rit, 1995) of the sigmoid function, $v_S = 10.69$ mV. If the PSP temporarily falls or rises beyond these limits, there is no further significant change in the firing rate.

The PSP of a NM can be decomposed into intrinsically and extrinsically caused components. While the latter is principally unlimited, the former is limited by the potential-to-rate operator of the presynaptic NM. Its range $[v_{ba,\min}, v_{ba,\max}]$ is $[0, 2e_{b0}c_{ba}H_{ba}\tau_{ba}]$ for excitatory and $[2e_{b0}c_{ba}H_{ba}\tau_{ba}, 0]$ for inhibitory inputs according to Eq. (4). Hence, extrinsically caused PSPs range effectively between $v_{b0} - v_S - v_{ba,\max}$ and $v_{b0} + v_S - v_{ba,\min}$. Extrinsic inputs beyond this range do not affect the system's behavior. This means that effective ranges for all three extrinsic inputs can be identified and translated into ranges of extrinsic input firing rates (see Table 1).[5]

Simulations of single neurons have shown that the dendritic time constants of the somatic response due to synaptic input for single neurons seem to vary between 4 and about 30 ms, depending on the distance between soma and synapse (Agmon-Snir and Segev, 1993; Gulledge et al., 2005). To ensure an inclusive treatment, we used the range of 2 to 60 ms; see also David and Friston (2003).

System analysis using bifurcation diagrams

Bifurcation diagrams show the asymptotically invariant behavior of a system by displaying the steady-state phase portrait, or a projection thereof, as a function of one or more system parameters. With smooth changes in these parameters, the dynamic behavior of the system may undergo sudden and drastic changes called bifurcations. Throughout this paper, we show codimension one bifurcation diagrams, which plot the asymptotic states of PSPs of the PCs (e.g., fixed points, limit cycles (LCs) or chaotic behavior evolving in time) against the extrinsic input on the PCs (see Fig. 2 and Figs. 10 to 13). To give an impression of the whole parameter space, we span planes of the dendritic time constants (Figs. 5, 7, and 9) and of the extrinsic inputs in INs (Figs. 6 and 8) using a classification of codimension one branches (see Fig. 4). An excellent treatment of the essentials of

[4] Because afferents from PCs on EINs and IINs are excitatory (i.e., $h_{23}(t) = h_{13}(t) = h_e(t)$), Eqs. (5) and (6) can be merged as follows: $v_{13}(t) = c_{13}v(t)$ and $v_{23} = c_{23}v(t)$ with $v(t) = (h_{23} \otimes m_3)(t) = (h_{13} \otimes m_3)(t)$.

[5] Note that only positive firing rates are biologically possible. In contrast, PSPs can be negative as well as positive, and induced by inhibitory as well as excitatory acting extrinsic afferents, respectively. Therefore, we use PSPs rather than firing rates to characterize extrinsic inputs.

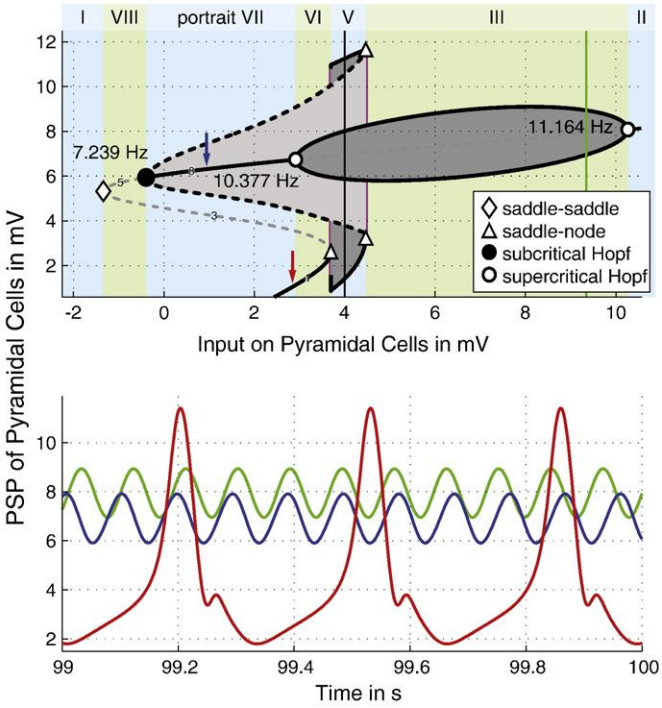

Fig. 2. Bifurcation diagram and exemplary solutions of Jansen's configuration ($v_{1T}=v_{2T}=0$, $\tau_e=10$ ms, $\tau_i=2\tau_e$). The diagram shows two telescoped branches of type I-B and II-AA (see Fig. 4). In the bifurcation diagram, solid lines represent stable and dashed lines unstable states. Branches of limit cycles correspond to gray regions bounded by solid lines for stable and dashed black lines for unstable limit cycles. Bifurcations are indicated by diamonds for saddle–saddle, triangles for saddle–node, black circles for subcritical Andronov–Hopf bifurcations, and white circles for supercritical Andronov–Hopf bifurcations. For all Andronov–Hopf bifurcations, the eigenfrequencies of the limit cycles that arise are indicated. The bifurcation diagram is stratified into equivalent states (green and blue bars) along the system parameter, that is, extrinsic input on pyramidal cells. The phase portraits according to each state are presented in Fig. 3. The purple lines indicate global bifurcations, here a saddle-node bifurcation in a Poincaré map occurring at the transition of state V–III and a Shil'nikov bifurcation (saddle-node) at the transition VI–V. Different extrinsic input levels on pyramidal cells (black and green vertical lines) result in different behavior depending on the past of a system's trajectory (blue and red arrows). For inputs of portrait V, the system produces sinusoidal oscillations (blue time series) starting from the blue and spiking activity (red series) starting from the red arrow. For inputs outside portrait V, the system is independent of the past, and produces sinusoidal oscillations (green series) within portrait III, for example.

bifurcation diagrams with special emphasis on their use for neuronal dynamics can be found in Breakspear and Jirsa (2007).

We create bifurcation diagrams to analyze the impact of extrinsic inputs and dendritic time constants on the system output, that is, the PSPs of the PCs, which are believed to be the main contributors to M/EEG. In the first step, we define the fixed point or equilibrium curve. The system can be expressed in vector form: $d\mathbf{Y}/dt=f(\mathbf{Y},\boldsymbol{\alpha})$, with the state vector $\mathbf{Y}=(v,\mathbf{u})^T$, where v is the seven-dimensional vector of the PSPs (see Eqs. (5) to (11)), and $\mathbf{u}$ is the vector of the derivatives of v and the parameter vector $\boldsymbol{\alpha}=(m_{1T}(t), m_{2T}(t), m_{3T}(t), \tau_e, \tau_i)$. The derivative state vector $d\mathbf{Y}/dt$ is a smooth function f of the system state vector $\mathbf{Y}$ and the system parameter vector $\boldsymbol{\alpha}$.

Fixed points

We obtain the fixed points $\mathbf{Y}_0$ by setting the derivatives to zero: $d\mathbf{Y}/dt=\mathbf{0}$. The coordinates of the fixed points cannot be expressed explicitly as a function of the extrinsic inputs. There is, however, a way to express the relationship between the system output (PSP of PCs) and the extrinsic input on PCs. We map $\mathbf{0}=f_0(\mathbf{Y}_0,\boldsymbol{\alpha}_0)$ to the PSP of the PCs $v_{3,0}(t)=v_{31}(t)+v_{32}(t)+v_{3T,0}(t)$. From Eqs. (5) to (11), it follows that the fixed points $v_{3,0}$ of the PSP of PCs can be defined in the $(v_{1T,0}, v_{2T,0}, v_{3T,0}, v_{3,0})$ space:

$$\begin{aligned} v_{3,0} &= \varepsilon_{31}c_{31}S_1\left(\varepsilon_{13}c_{13}S_3\left(v_{3,0}\right)+v_{1T,0}\right) \\ &\quad+\varepsilon_{32}c_{32}S_2\left(\varepsilon_{23}c_{23}S_3\left(v_{3,0}\right)+v_{2T,0}\right)+v_{3T,0}, \end{aligned} \tag{13}$$

where $v_{bT}=\varepsilon_{bT}c_{bT}m_{bT}$ with $b=\{1,2,3\}$ and $\varepsilon_{ba}=H_{ba}\tau_{ba}$, $\tau_{ba}=\{\tau_e,\tau_i\}$ with $a=\{1,2,3\}$. This equation can be solved for the extrinsic input v_{3T} on PCs as a fixed point curve function of the extrinsic inputs on INs and the PSP of the PCs, yielding a unique mapping that can be used for the analytical computations. Note that, as described above, the $\varepsilon_{e,i}$ are constant. Hence, the shape of the fixed point curve only depends on the extrinsic inputs to the INs, but not on the dendritic time constants.

Every fixed point is completely determined algebraically in the state space by the fixed point term $v_{3,0}$ of the PSPs of the PCs, $\mathbf{Y}_0=f_0(v_{3,0}, m_{1T,0}, m_{2T,0}, m_{3T,0})$ with:

$$Y_0=\begin{bmatrix} \varepsilon_{13}c_{13}S_3\left(v_{3,0}\right) \\ \varepsilon_{23}c_{23}S_3\left(v_{3,0}\right) \\ \varepsilon_{31}c_{31}S_1\left(\varepsilon_{13}c_{13}S_3\left(v_{3.0}\right)+\varepsilon_{1T}c_{1T}m_{1T.0}\right) \\ \varepsilon_{32}c_{32}S_2\left(\varepsilon_{23}c_{23}S_3\left(v_{3.0}\right)+\varepsilon_{2T}c_{2T}m_{2T.0}\right) \\ \varepsilon_{1T}c_{1T}m_{1T,0} \\ \varepsilon_{2T}c_{2T}m_{2T,0} \\ \varepsilon_{3T}c_{3T}m_{3T,0} \\ \mathbf{0}_{7\times1} \end{bmatrix} \tag{14}$$

where $\mathbf{0}_{7\times1}$ is the seven-dimensional zero vector. In the second step, the behavior near the fixed points can be studied by linearizing the 14-dimensional system and evaluating its Jacobian at the fixed points (Eq. (14)). By analyzing the eigenvalues of the Jacobian, we are able to specify local stability properties like stable or unstable nodes, foci or saddles. Since there is no explicit form for the eigenvalues of the Jacobian as function of the extrinsic input on the PCs, the eigenvalues were computed for 10^4 equally spaced points. Note that the Jacobian depends on the extrinsic inputs as well as on the dendritic time constants. This means that, for any particular extrinsic input configuration, although the fixed point curve is constant in the 14-dimensional state space, the behavior in the vicinity of the fixed points varies with the dendritic time constants. System stability changes if at least one eigenvalue of the system crosses the imaginary axis. Points with zero real part(s) are called critical or nonhyperbolic fixed points, indicating possible *local* bifurcations.

Bifurcations

For identifying bifurcations, we first locate the critical points using the Nelder–Mead simplex method (Nelder and Mead, 1965). Second, the bifurcations are classified using the mathematical theory of codimension one bifurcations (Kuznetsov, 1998; Perko, 2001). We distinguish between the Andronov–Hopf (AH) and saddle bifurcation families. AH bifurcations occur if a change in the investigated system parameter (in our case the extrinsic input to the PCs) causes two complex conjugate eigenvalues to cross the imaginary axis (i.e., the real part changes from positive to negative or vice versa). In this case, LCs can arise. According to the first-order Lyapunov exponent, we differentiate between supercritical and subcritical AH bifurcations; in the first case, the LCs are stable, otherwise they are unstable. The saddle bifurcation family occurs if at least one (but not all) eigenvalue crosses the imaginary axis so that the eigenvalues in at least one of the two states have both negative and positive real parts. According to the leading eigenvalue (which plays an important role, especially for Shil'nikov's homoclinic bifurcations present in our dynamics), the counterpart state could be of three types, leading to the definition of three types of saddle bifurcations. For saddle–node bifurcations, all

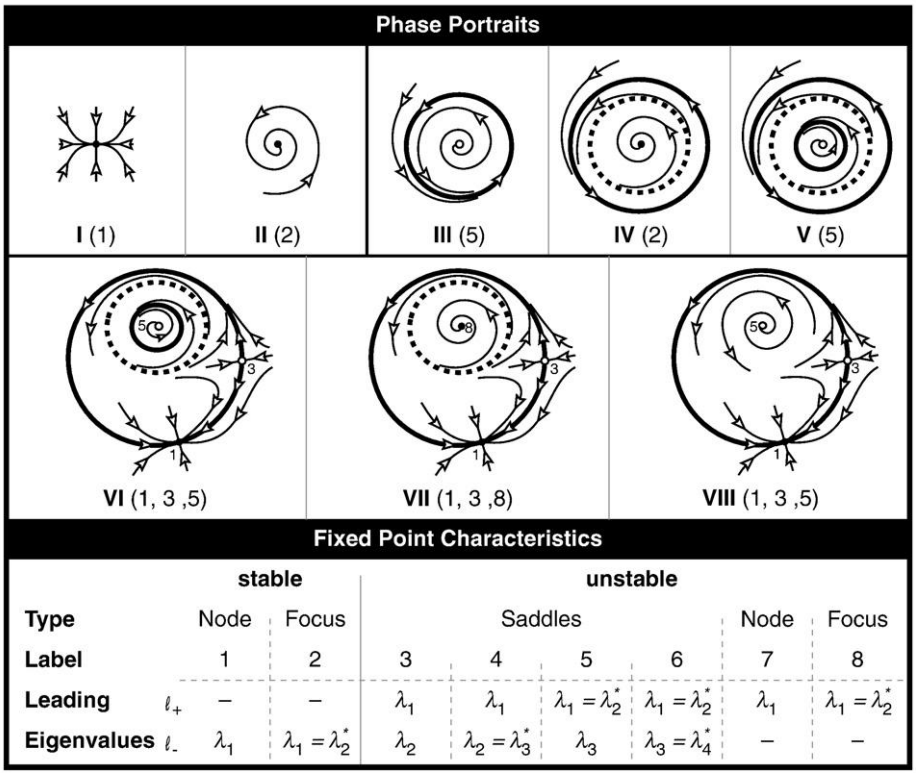

Fig. 3. Schematic phase portraits representing the qualitative system states in bifurcation diagrams. Note that these phase portraits display the principal features in a plane according to the leading eigenvalues, while the actual phase portraits live in a 14-dimensional space. The displayed cases are referenced in the bifurcation diagrams in Figs. 2 to 5. Phase portraits I and II show stable fixed points, portraits III–V are due to Andronov–Hopf bifurcations and portraits VI–VIII are possible combinations of these, and lead to heteroclinic cycles. Portrait I is a stable node and II is a stable focus. Phase portrait III consists of one stable limit cycle. Phase portraits IV and V are similar to III, but with more than one limit cycle: one stable and one unstable limit cycle in IV and two stable and one unstable limit cycle in V. Phase portraits VI–VIII comprise heteroclinic cycles due to the coexistence of a saddle and a node. The limit cycles in VI and VII as well as the unstable focus in VIII force the system to connect unstable and stable manifolds of the saddle and node stabilities, that is, to produce heteroclinic cycles. The fixed points in the phase portraits are characterized with respect to the leading eigenvalues, which play an important role, especially for the Shil'nikov bifurcations that we have. The eigenvalues with positive (resp. negative) real parts that are closest to the imaginary axis are called the unstable ℓ_+ (stable ℓ_-) leading eigenvalues.

real parts of the hyperbolic eigenvalues have the same sign and the crossing eigenvalues (nonhyperbolic) are real-valued. If all real parts of the hyperbolic eigenvalues have the same sign and the crossing eigenvalues are complex conjugate, one speaks of a saddle–focus bifurcation. Finally, if the hyperbolic eigenvalues still have both negative and positive real parts, the bifurcation is of the saddle–saddle type, meaning that the topology of the saddle and not its stability changes. In general, a saddle-saddle bifurcation refers to the situation where two saddles of different types collide and vanish. All bifurcations are checked for their genericity.[6] For testing saddle bifurcations for homoclinic orbits, called Shil'nikov bifurcations (Glendinning and Sparrow, 1996; Kuznetsov, 1998; Shil'nikov, 1969), and for further *global* bifurcations, we used the continuation package *Cl_MatCont* for MatLab™ by Govaerts, Kuznetsov et al. (available at http://www.matcont.ugent.be/). The term global refers to the fact that the trajectory not only depends on the local properties in the vicinity of the fixed point.

In the last step, the bifurcation analysis is completed by the identification of the branches of LCs arising from local and global bifurcations. Accordingly, we continued the bifurcating LCs away from the bifurcation points. The initial periodic solutions from which we were able to initialize the LC continuations were taken from the bifurcation points. For this purpose, we also used the package *Cl_MatCont* (http://sourceforge.net/projects/matcont/).

Finally, we create bifurcation diagrams comprising fixed points, stabilities, local as well as global bifurcations, branches of LCs and schematic phase portraits representing each state. As an example, Fig. 2 shows the bifurcation diagram of the standard parameter configuration proposed by Jansen and Rit (1995). The dynamic behavior for a specific parameter value can be illustrated by schematic phase portraits (see Fig. 3). These phase portraits show transient and steady-state trajectories in a two-dimensional subspace of the state space in a qualitative way. One can recognize oscillatory and nonoscillatory dynamics in the vicinity of fixed points and LCs, as well as heteroclinic orbits (see Fig. 3 for further details).

A systematic classification of LC branches

In our analysis, various topological arrangements of branches of LCs for varying input occurred. We qualitatively classified them into several types, which are characterized by nested, alternately stable and unstable LCs, separated by stability-changing global bifurcations. A comprehensive chart of all (globally) stable branches in the projection plane (v_{3T}, v_3) is shown in Fig. 4. First, we classified branches as principal types according to the number of AH bifurcations involved, indicated by Roman numerals. We only found branches involving either one or two AH bifurcations (principal types I and II). We further classified a branch more precisely according to its number of LC-stability-changing global bifurcations. Starting from a particular AH bifurcation, we counted the number of such global bifurcations, indicated by capital letters. For example, branches

[6] Eigenvalues reveal critical fixed points at which bifurcations could exist. However, the generation of a bifurcation at such a critical fixed point depends on nondegeneracy and transversality conditions, the so-called genericity conditions (Kuznetsov, 1998). These conditions are inequalities involving partial derivatives of f with respect to $\mathbf{Y}$, v_{1T}, v_{2T}, and v_{3T}, evaluated at the nonhyperbolic fixed point.

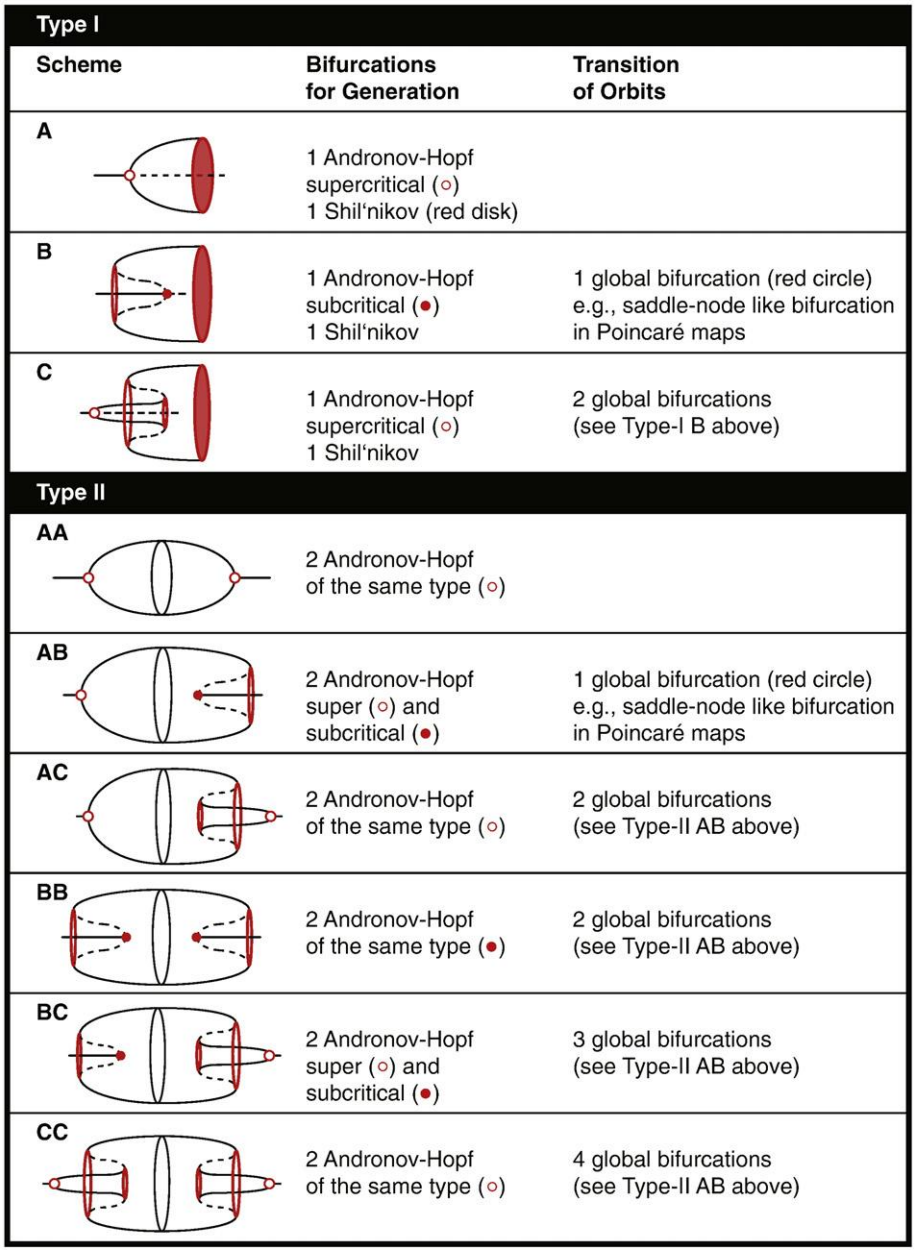

Fig. 4. Classification of the globally stable branches of limit cycles. Principal type I or II was classified according to the number of involved Andronov–Hopf bifurcations (one or two). The number of global bifurcations (red circles) that change the stability of the limit cycles is indicated by capital letters (A to C). Each global bifurcation is assigned to a local Andronov–Hopf bifurcation by the shortest distance on the fixed point curve. Fundamental frequencies of limit cycles of branch type II-AA are relatively stable because the orbit is generated by Andronov–Hopf bifurcations only. On the other hand, the oscillation frequencies vary across a broad range for all branches of type I due to the involved Shil'nikov bifurcation. Sinusoidal or harmonic oscillations are exclusively produced in the limit cycle branch type II-AA and anharmonic (spiky) oscillations are exclusively produced by branch type I-B and II-BB. All other branch types produce both oscillations.

was classified as A, B, or C with no, one, or two stability-changing global bifurcations, respectively. For branches of type II, each global bifurcation was assigned to either of the two AH bifurcations (e.g., label AC for a type II branch means that one AH bifurcation is not associated with any LC-stability-changing global bifurcation, while the other AH bifurcation is associated with two global bifurcations). The association of AH to global bifurcations was based on the shortest distance to the fixed point curve. We found branches with a maximum of two stability-changing global bifurcations (labeled C). Several LCs coexist for the same parameter set if (i) the corresponding branches are of type B or higher (see Fig. 4), (ii) branches are encapsulated in one another (see, e.g., Fig. 10 for a II-AA branch encapsulated into a II-AB branch), or (iii) branches are telescoped into each other (see, e.g., Fig. 11 for a II-AA branch telescoped into a II-AB branch). In the latter case, at least one global bifurcation (which changes the LC-stability) of one branch is in range of another branch.

Results

As a first step, we analyzed the standard configuration proposed by Jansen and Rit (1995) with no extrinsic input from other cortical and subcortical areas on the INs ($v_{1T}=v_{2T}=0$, $\tau_e=10$ ms, $\tau_i=2\tau_e$). This is mostly a replication of the work of Grimbert and Faugeras (2006), but we found an additional bifurcation that has not been reported before. Then, we systematically scanned the five-dimensional parameter space spanned by the extrinsic input levels and the inhibitory/

excitatory dendritic time constants (see Table 2 for values used), computing a bifurcation diagram of the fifth parameter and the extrinsic input level to the PCs for each point in that space. In terms of steady-state dynamic behavior, we observed two different basic oscillatory regimes, which would be reflected in M/EEG: low-amplitude sinusoidal oscillations caused by AH bifurcations (referred to as *harmonic oscillations* throughout this work) and high-amplitude *anharmonic* (spike-like) *oscillations* caused by global bifurcations such as of Shil'nikov type. We further characterized these phenomena, in particular by determining the frequencies and amplitudes of the oscillations generated as well as their stability with respect to varying system parameters and by considering the transitions between different oscillatory regimes through bifurcations. We used the classification scheme of the stable LC branches introduced above (see Materials and methods) to map the incidence of these topologies as well as the associated oscillatory regimes to the parameter space. Finally, we present some representative configurations revealing new behavior which is potentially biologically interesting.

Bifurcation diagram for the parameter configuration of Jansen and Rit

We analyzed the standard configuration of the NMM according to Jansen and Rit (1995), reproducing and extending the results obtained by Grimbert and Faugeras (2006). See Fig. 2 for the bifurcation diagram. Fig. 3 shows the associated phase portraits, schematically illustrating the trajectories for the different regions of the bifurcation diagram. In accordance with Grimbert and Faugeras (2006), we found one subcritical and two supercritical AH bifurcations, a homoclinic saddle–node (Shil'nikov) and a global bifurcation. The two supercritical AH bifurcations cause a branch of type II-AA (Fig. 4), producing sinusoidal oscillations around 10.8 Hz, which might serve as a theoretical basis for alpha rhythm generation, as suggested by Jansen and Rit (1995). The subcritical AH bifurcation produces a branch of type I-B (Fig. 4) featuring unstable LCs, and the saddle–node bifurcation causes stable homoclinic LCs with a fundamental frequency ranging between 0.1 Hz and 4.6 Hz, which could be used for modeling epilepsy-like spiking activity (see, e.g., Marten et al., 2009; Suffczynski et al., 2005; Wendling et al., 2002, 2000). Both stable homoclinic and unstable LCs collide and vanish through a global bifurcation (saddle–node bifurcation in Poincaré maps).

In addition to these results, we found a local saddle–saddle bifurcation that was not reported in the work of Grimbert and Faugeras (2006). This type of bifurcation does not represent a change in stability (i.e., lying within an unstable section of the fixed point curve) but a topological change of the saddle, in this case caused by complex conjugate eigenvalues. In particular, this bifurcation indicates that the system produces unstable oscillations for low-amplitude inhibitory extrinsic input on PCs (i.e., lying on the section of the fixed-point curve between this local saddle–saddle bifurcation and the subcritical AH bifurcation, see Fig. 2), due to the unstable focus in the corresponding phase portrait VIII in Fig. 3. Just like the saddle family of bifurcations in general, saddle–saddle bifurcations are, in principle, able to cause homoclinic LCs (Shil'nikov saddle–saddle bifurcation). However, in this case, no homoclinic LCs could be found using the Cl_MatCont package.

Extrinsic inputs and dendritic time constants—mechanisms for oscillations

Next, we analyzed the extended model of a cortical area by considering nonzero constant extrinsic input levels, $v_{1T}(t)$, $v_{2T}(t)$, and $v_{3T}(t)$, on all three NMs, and by systematically varying these inputs as well as the dendritic time constants τ_e and τ_i. Therefore, we captured a five-dimensional parameter space (see Table 2 for discretizations) by computing a bifurcation diagram of the PSPs of the PCs against the extrinsic input v_{3T} on the PCs for each combination of the remaining four parameters. The configuration of Jansen and Rit, as described above, represents only one particular case in this analysis.

Generally, we found two basic mechanisms for generating oscillations: AH bifurcations and Shil'nikov bifurcations. For AH bifurcations, one can compute eigenfrequencies. Although, in a strict sense, these frequencies apply only to the bifurcation point, they nevertheless give a good approximation for the oscillation frequencies of LCs at some distance in adjacent branches. In contrast, Shil'nikov, or more generally speaking, global bifurcations, usually do not offer such indications of oscillation frequencies because of the global dependencies, which are not reflected by the local eigenvalues. Upon passing Shil'nikov bifurcations, the homoclinic LCs suddenly arise at high amplitudes. The oscillation frequency is zero at the bifurcation point and greatly increases with increasing distance. Thus, in response to variations of the extrinsic input level to the PCs, the fundamental oscillation frequency is relatively constant for AH–LCs (*harmonic oscillations*) and quite variable for Shil'nikov's homoclinic cycles (*anharmonic oscillations*).

Upon passing the AH bifurcation, the harmonic oscillations emerge gradually. Variations in the extrinsic input to the PCs (e.g., noise) result in some variations in amplitude and only small variations in frequency. This gives rise to waxing and waning oscillations of relatively stable frequency, as, for example, observed in EEG alpha waves. In contrast, upon passing a Shil'nikov bifurcation, highly anharmonic (i.e., spike-like) oscillations appear suddenly with high amplitude and low frequency (initially zero). Temporal variations in the extrinsic input to the PCs lead to moderate amplitude and drastic frequency changes. As a result, quite irregular (when using noisy inputs) anharmonic oscillations that resemble M/EEG phenomena during epileptic seizures[7] appear (see, e.g., Marten et al., 2009; Suffczynski et al., 2005; Wendling et al., 2002, 2000). Overall, we found fundamental frequencies ranging between 0.1 Hz and 79.6 Hz, which covers the bulk of relevant frequency bands in M/EEG.

Conditions for harmonic and anharmonic oscillations

In Figs. 5 and 6, the occurrence frequencies of the various branch types (see Fig. 4) are plotted against the system parameters. The dynamics of the AA branches caused by two supercritical AH bifurcations are by far the most common phenomena (comprising about 77% of all investigated loci in parameter space where stable LCs occur). In particular, this type of behavior occurs in configurations with approximately equal inhibitory and excitatory dendritic time constants in combination with extrinsic excitatory input on the IINs of less than 8 mV (250 spikes/second[8]), and with extrinsic input on the EINs of either less than about −17 mV (i.e., inhibitory; more than 39 spikes/second) or more than about 8 mV (i.e., excitatory; more than 250 spikes/second). Experimentally, spontaneous average spike rates mostly do not exceed 10 Hz (in rats; e.g., Attwell and Laughlin, 2001; Nawrot et al., 2007), but activity related rates can be as high as 80 Hz (see, e.g., Shenoy et al., 2003, for activity of premotor neurons in monkeys). This suggests that, in our model, the AA branch behavior depends on a rather strong inhibition of the EINs. If the inhibitory dendritic time constant is larger than 1.3 times the excitatory one and the extrinsic input to the EINs lies between about −17 and 8 mV (i.e., inhibitory input of less than 39 or excitatory input of less than 250 spikes/second), branches of type II-AB occur, allowing both harmonic and highly anharmonic (often spike-like) oscillations. This scenario is more compatible with the typical moderate spike rates observed experimentally. If the inhibitory

[7] It should be pointed out that, in general, all types of limit cycles can degenerate due to the nonlinearity and surjection (global shape) of the fixed point curve.

[8] The transformation from PSP to spike rate is done by division by the respective product of average synaptic gain and dendritic time constant $H_{e,i} \cdot \tau_{e,i} = \varepsilon_{e,i}$. See Materials and methods section.

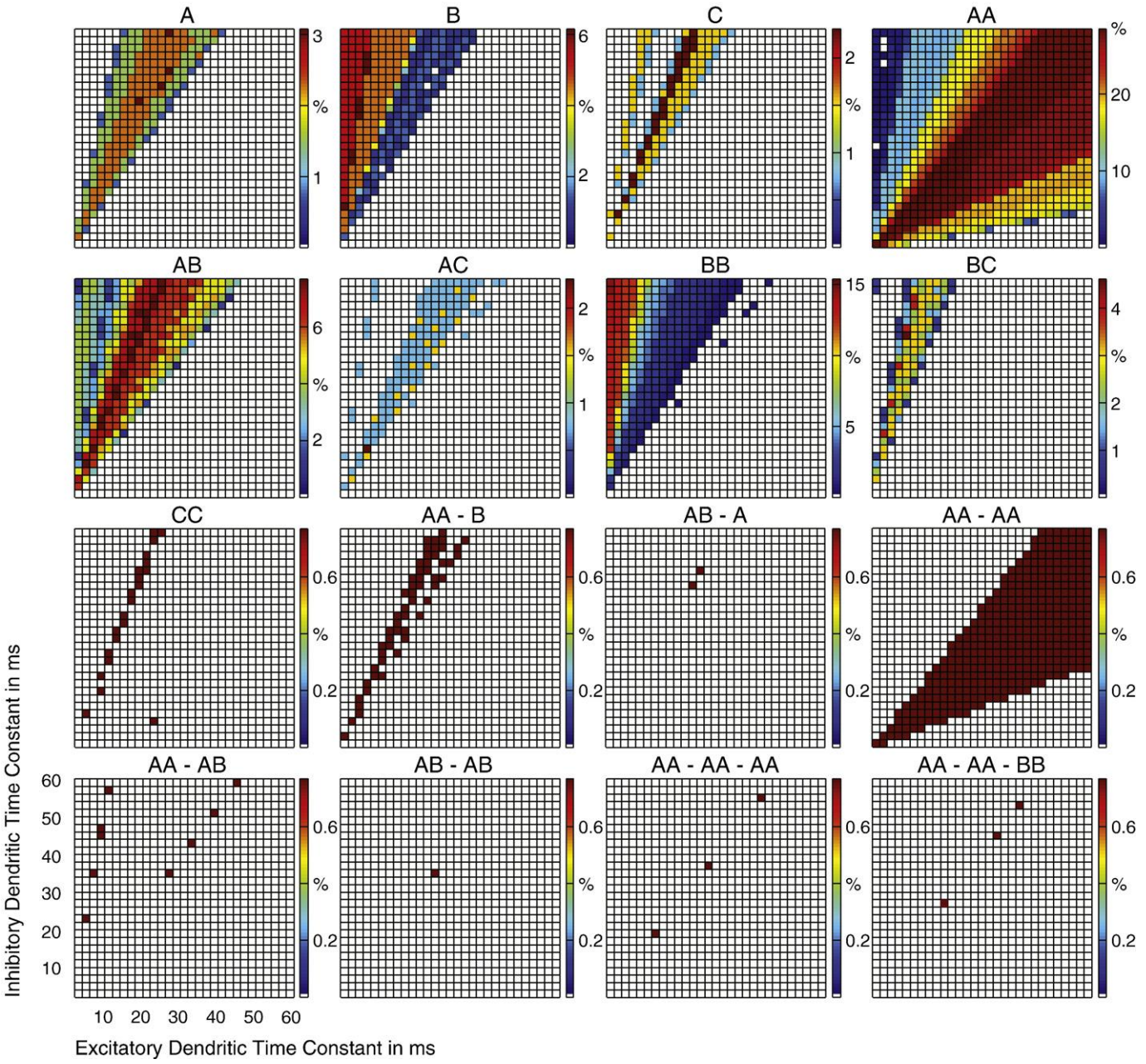

Fig. 5. Occurrence of branch types projected in the plane of the dendritic time constants. The most frequent branch type is II-AA, with 76.7%, followed by type II-AB (7.7%), II-BB (6.8%), I-B (4.2%), I-A (1.9%), II-BC (1.1%), I-C (1%), II-AC (0.6%), and II-CC (0.1%). Branches of type II-AA exist for parameter configurations with dendritic time constant ratios $\tau_i/\tau_e > 0.2$, most frequently around ratios of 1. For increasing ratios, other branch types appear in the order: II-AB (>1.3, most frequently ≈2.4), II-AC (1.4–5.0 scattered), I-A (1.44–4.0), I-B as well as II-BB (>1.6, most frequently >3), I-C (1.7–5 scattered, most frequently ≈2.4), II-CC (≈2), and II-BC (2.6–6.0). Combinations of branch types (1.7% of all of all configurations where stable limit cycles occur) and branch type II-CC occur rarely (singular phenomena). The standard configuration according to Jansen and Rit ($v_{1T} = v_{2T} = 0$, $\tau_e = 10$ ms, $\tau_i = 2\tau_e$) is such a special case since it consists of branches of type I-B and II-AA. For the classification of branch types, see Fig. 4.

dendritic time constant is approximately three times larger than the excitatory one, BB (only anharmonic oscillations) or B branches appear with predominantly spiking activities. In our model, other branch types, in particular combinations of the basic types, cover only small portions of the parameter space. For example, the specific branch combination corresponding to the standard configuration of Jansen and Rit (AA-B) is restricted to input to IINs between 0 and 2 mV (i.e., excitatory input of less than 62 spikes/second), input to EINs between −4 and 4 mV (i.e., inhibitory input of less than 9 or excitatory input of less than 125 spikes/second) and inhibitory dendritic time constants about twice that of the excitatory ones. Note that the translation from PSP to spike rate depends on the assumed products of dendritic time constant and synaptic gain, which we set to the values proposed by Jansen and Rit (1995). Moreover, the resulting spike rates represent the mean *input* rates of the respective NMs, which relate to the firing rates of the presynaptic neurons by the connectivity constants ($m_{bT} = c_{bT} \cdot m_T$, $b = \{1, 2, 3\}$). These were set to 1 in our analysis, with the assumption that, on average, each presynaptic neuron contacts one postsynaptic one. Other values for the connectivity constants would lead to an according scaling of the firing rates.

LC branches of type II-AA provide harmonic oscillations with relatively stable fundamental frequencies because the orbit is only generated by AH bifurcations. In contrast, due to the Shil'nikov bifurcation involved in all branches of type I, the oscillation

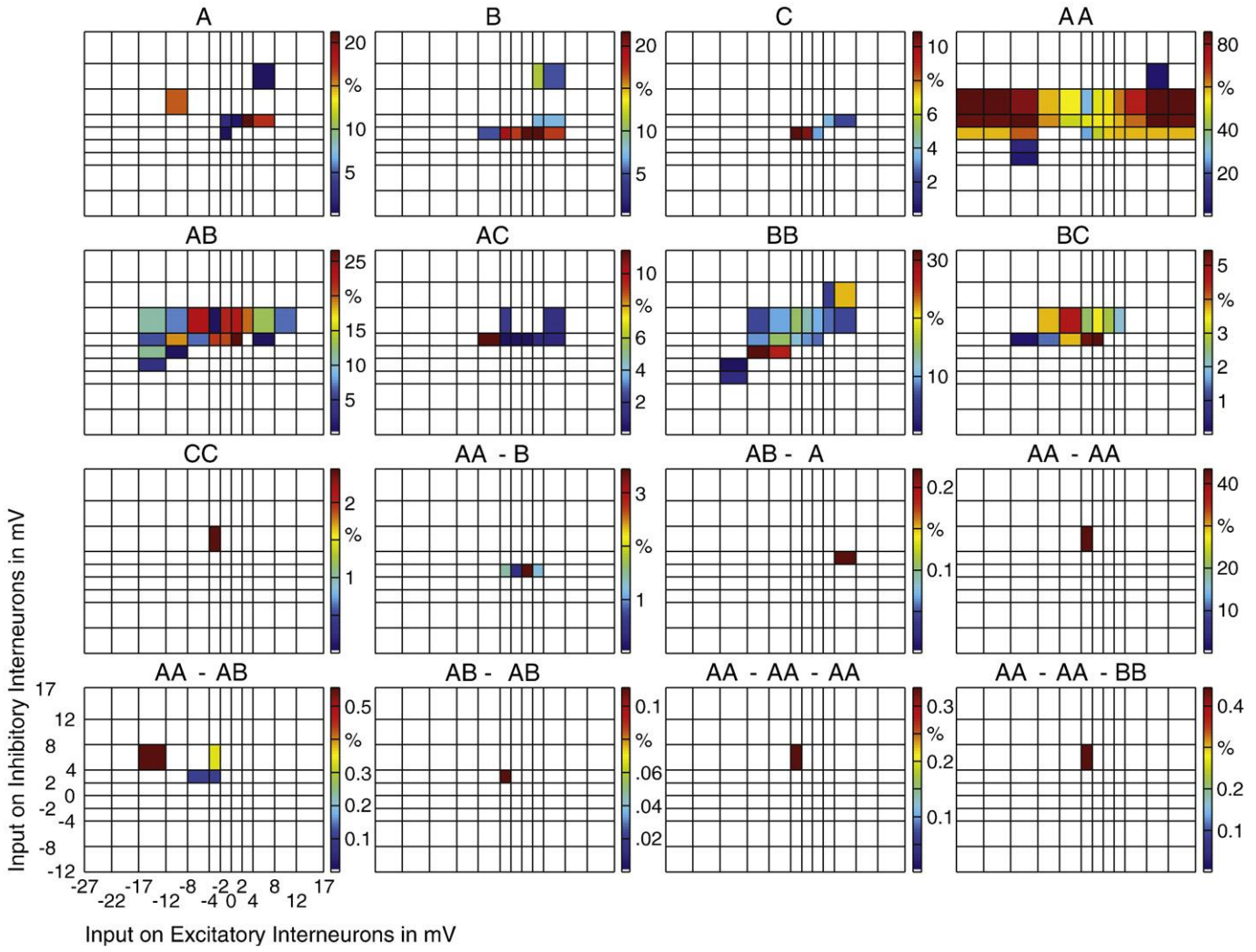

Fig. 6. Occurrence of branch types projected to the plane of the extrinsic input on interneurons. Limit cycle branches of type II-AA are most frequent for configurations with extrinsic excitatory input on the inhibitory interneurons of less than 8 mV and with extrinsic input on the excitatory interneurons of either less than about −17 mV (i.e., inhibitory) or more than about 8 mV (i.e., excitatory). Between −17 and 8 mV, most branches of type II-AA pass over to branches of type II-AB, II-BB and/or I-B. Most limit cycle branches occur for excitatory input on inhibitory interneurons. Branches of type II-AA arise independently of the extrinsic input on excitatory interneurons, but all other types and combinations of branches arise focally for a certain range. This means that extrinsic input on excitatory interneurons causes most II-AA branches to turn into more complex branches and combinations. The projection also reveals that combinations of branch types and branches of type II-CC are quite rare and local. The dominant combination of branches is II-AA, with 83.2%, followed by AA-B (12.5%), AA-AB (2.1%), AA-AA-BB (0.9%), AA-AA-AA (0.6%), AB-A (0.4%), and AB-AB (0.2%). See Fig. 4, for the classification of branch types.

frequencies vary across a broad range of values. The frequency ranges of all other branch types are dependent on the involved global bifurcations that change the stability of the LCs and generate anharmonic oscillations.

Figures 7 and 8 provide an overview of the circumstances under which the system produces harmonic and anharmonic (spiky) oscillations. In general, either type of oscillations is only possible if the dendritic time constant of the inhibitory synapses between INs and PCs is not too short compared to one of the excitatory synapses: $\tau_i \geq 0.2\tau_e$ (see Fig. 7). Since the effective dendritic time constant increases with the average distance between synapses and soma (e.g., Gulledge et al., 2005), this means that, especially with excitatory input to very distal dendritic branches, there must be inhibitory synapses with rather large time constants to render the system capable of oscillating. The dendritic time constants also have a profound influence on the type and frequency of the oscillations that can be produced. If $\tau_i \geq 1.3\tau_e$, the system may (depending on the extrinsic inputs and the initial conditions) produce high-amplitude anharmonic oscillations. Otherwise, only harmonic oscillations are generated, the frequency of which depends on the dendritic time constants in a systematic way; see Fig. 9 for examples. In general, we found that the period of stable LCs increases with the dendritic time constants. In extension of the simulation-based frequency analysis of David and Friston (2003), we identified the generating mechanisms for the oscillations.

For the standard configuration of Jansen and Rit (1995), the parameter range where David and Friston (2003) identified harmonic oscillations can be divided into two regions. For relatively short inhibitory dendritic time constants ($\tau_i \leq 0.2\tau_e$), we find stable foci instead of stable LCs, and therefore the system can only oscillate in the presence of constant perturbing extrinsic input, for example, noise. In contrast, if the inhibitory dendritic time constant is larger ($\tau_i \geq 0.2\tau_e$), stable LCs occur and the system oscillates autonomously, even with constant input. In particular, the anharmonic oscillations referred to as *hypersignals* by David and Friston are revealed to be caused by LCs due to global bifurcations. Generally, bifurcation analysis offers a way to distinguish between intrinsic oscillations (stable LCs) and extrinsically driven oscillations (e.g., noise-driven stable foci).

With respect the extrinsic inputs on INs, Fig. 8 gives an overview of the conditions of occurrence for oscillations. Clearly, the system

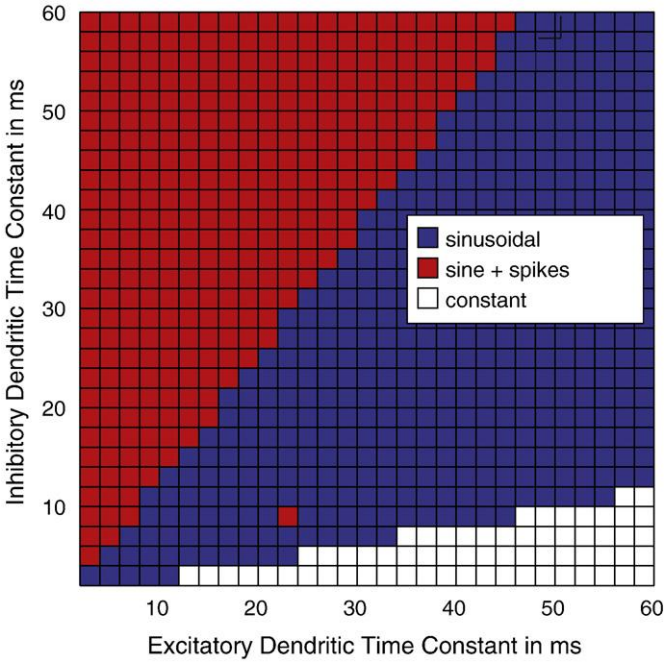

Fig. 7. Existence of limit cycles mechanisms depending on dendritic time constants. Blue: sinusoidal or harmonic oscillations due to Andronov–Hopf bifurcations, red: sinusoidal and anharmonic (spiky) oscillations caused by global bifurcations like of Shil'nikov's type. The diagram is a projection of the entire parameter space onto the plane of the dendritic time constants. No limit cycles occur for dendritic time constant ratio $\tau_i/\tau_e \leq 0.2$. Limit cycles occur for 24% of all configurations in the parameter space. For ratios > 0.2, parameter configurations with Andronov–Hopf cycles exist, and further, for ratios > 1.3, configurations containing both harmonic and anharmonic oscillations exist.

only oscillates if the IINs are not inhibited and are not excited above about 8 mV (with few exceptions). Moreover, anharmonic oscillations are limited to extrinsic inputs on the EINs between approximately −17 mV (i.e., inhibition of the INs) and 8 mV (i.e., excitation of the INs).

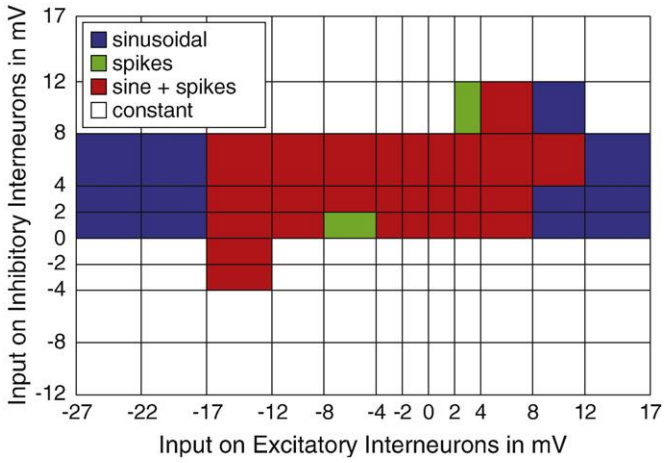

Fig. 8. Existence of limit cycle mechanisms depending on extrinsic inputs. Blue: sinusoidal or harmonic oscillations due to Andronov–Hopf bifurcations, green: anharmonic to spiky oscillations caused by global bifurcations like of Shil'nikov's type, red: both types of oscillations. The diagram is a projection of the entire parameter space onto the plane of the extrinsic inputs. Extrinsically inhibited inhibitory interneurons induce no limit cycles (with some exceptions). Limit cycle branches, especially with harmonic oscillations, mainly occur for extrinsically excited inhibitory interneurons (up to roughly 8 mV) for all extrinsic inputs on excitatory interneurons. In contrast, extrinsic input on excitatory interneurons is relevant for the occurrence of anharmonic oscillations (approximately between −17 and 8 mV).

Example configurations illustrating potential applications

In this section, we will describe four example configurations using their bifurcation diagrams. They have been selected to illustrate interesting transitional behavior between oscillatory regimes, which may be potentially relevant for modeling the brain processes underlying real M/EEG phenomena, such as ordered sequences of dynamic regimes (for modeling sequences in epilepsy by using thalamocortical models see, e.g., Marten et al., 2009; Rodrigues et al., 2009; Suffczynski et al., 2005).

The first example is presented in Fig. 10. It shows the system behavior for extrinsically inhibited EINs and excited IINs ($v_{1T} = -4$ mV and $v_{2T} = -v_{1T}$) and high dendritic time constants ($\tau_e = 26$ ms and $\tau_i = 34$ ms), which correspond approximately to the upper limit of the physiologically plausible range (see Materials and methods section for ranges of the system parameters). This example demonstrates the simultaneous existence of more than one LC branch for the same parameter range that means an unstable branch of type II-AA, which is encapsulated in a branch of the same type but of opposite stability. Such stable II-AA-AB branches make up about 2% of all observed multibranch configurations (see Figs. 5 and 6). The unstable AH–LCs act as separatrix,[9] which separates two system modes of behavior (here unstable from stable LCs). If the system is initialized inside the unstable AH–LCs, it will produce constant output, or, in the presence of low-amplitude perturbations, damped oscillations (idle mode). If the system is then perturbed beyond the separatrix, it suddenly enters an excitation mode and produces anharmonic oscillations. This mechanism also works in the opposite way, from excitation to idle mode. However, the interesting feature is that this transition behavior is generally irreversible; that is, the system will not revert to its original mode even after the perturbing stimulus is gone. Such switching behavior in response to a brief stimulus is characteristic of many normal and pathological processes in the brain, such as redirection of attention by a relevant sound or touch, waking up by salient stimulation, or epileptic seizures elicited by sudden, unexpected stimuli (startle epilepsy).

The second example in Fig. 11 shows a case with still stronger inhibition of the EINs and short dendritic time constants for the excitatory synapses ($v_{1T} = -17$ mV, $v_{2T} = 4$ mV, $\tau_e = 4$ ms, $\tau_i = 5.5\tau_e$). The bifurcation diagram reveals overlapping but separate branches, which provide three LCs for the same parameter setting: a branch of type II-AA which is shifted into a branch of type II-AB (with about 2% occurrence, where 20% of these are telescoped). This configuration features both sudden and continuous entering into LCs as well as sudden changes between them. The system traverses states (branches) in qualitatively different ways for increasing and decreasing extrinsic input on PCs. For instance, the system suddenly switches from idle mode (stable focus in phase portrait IV with initialization indicated by the blue arrow and an input level of about 56 mV) to excitation mode (high-amplitude anharmonic oscillations) for increasing input (exceeding about 64 mV) by passing the subcritical AH bifurcation (switching the phase portrait from type IV to III). It remains in the excitation mode even after cessation of the input perturbation (potential back to 56 mV), thus seeming to provide a mechanism for irreversible change caused by a transient input perturbation (see previous example). Additionally, the system may change suddenly from one excitation mode (anharmonic oscillations) to another (harmonic oscillations) for decreasing inputs (below about 54 mV) by passing a global bifurcation (changing the phase portrait from type V to III). If the input to the PCs then returns to the original

[9] A separatrix marks a boundary between trajectories with different properties.

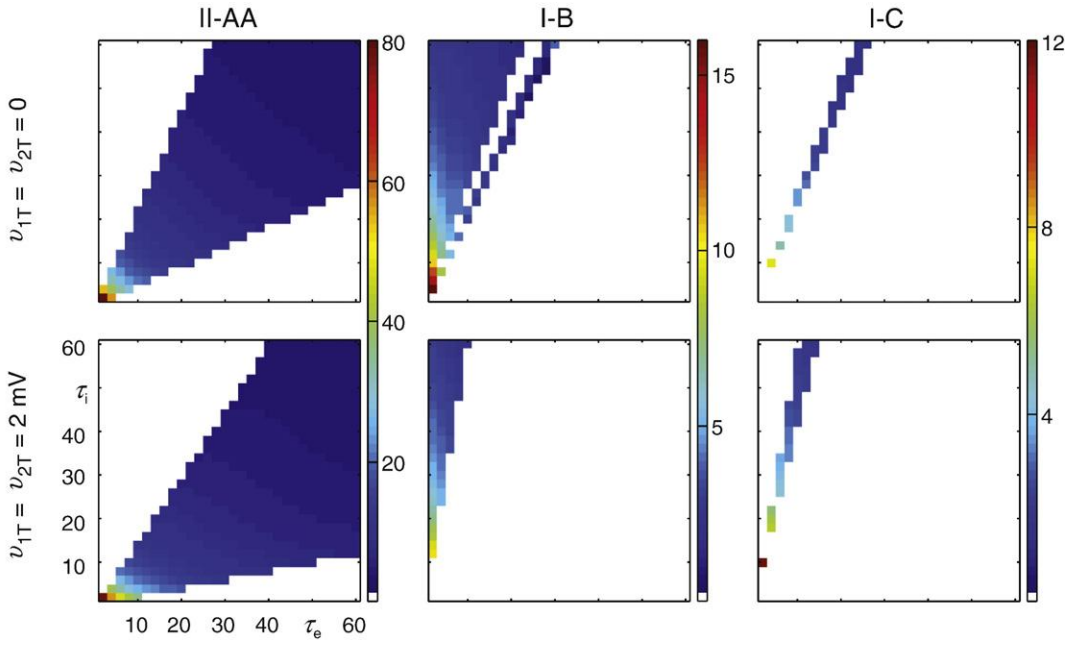

Fig. 9. Frequency charts of limit cycle branches. For two configurations of extrinsic inputs on interneurons (rows) depending on the excitatory and inhibitory dendritic time constants (τ_e and τ_i), we see the carts of branch type II-AA, I-B, and I-C (columns). The standard configuration according to Jansen and Rit can be found in the first row ($v_{1T} = v_{2T} = 0$, $\tau_e = 10$ ms, $\tau_i = 2\tau_e$). The oscillation frequency values of limit cycles in branches of type II-AA represent mean values over Hopf cycle range and single values for type I branches (constant distance in relation to Shil'nikov bifurcations). For the classification of branch types see Fig. 4.

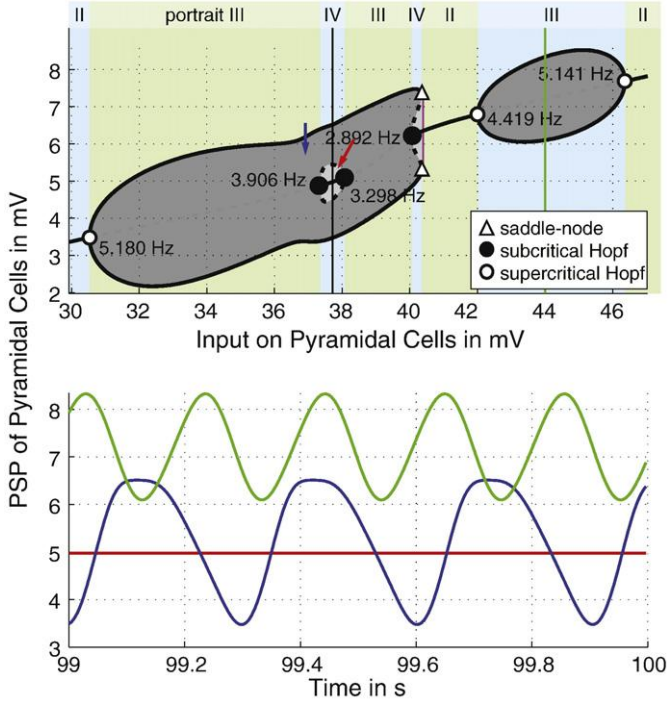

Fig. 10. Encapsulated limit cycle within another limit cycle of opposite stability (for parameter configuration $v_{1T} = -4$ mV, $v_{2T} = -v_{1T}$, $\tau_e = 26$ ms, $\tau_i = 34$ ms). Here, we see an unstable II-AA branch, which exists within a stable branch of type II-AB and a II-AA branch. For the explanation of the bifurcation diagram, see the legend of Fig. 2. If the system were initialized outside the branches of unstable limit cycles (blue arrow), the system would tend to produce transient anharmonic oscillations (blue time course) in the parameter range of stable limit cycles (indicated by the black line within state IV). Otherwise, the system would generate constant output (red arrow and red time course) but may suddenly switch to sinusoidal activities if moved over the separatrix by any perturbation.

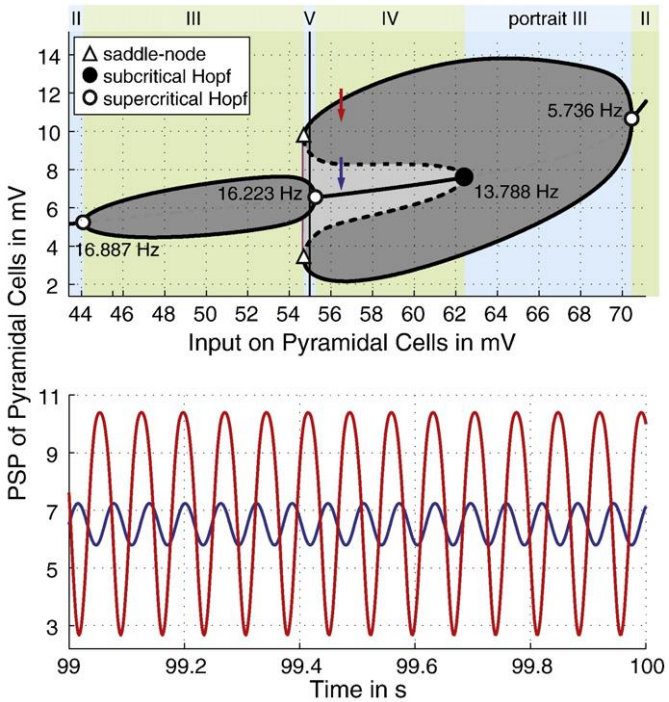

Fig. 11. Overlapping branches of limit cycles provide two stable limit cycles for the same parameter configuration ($v_{1T} = -17$ mV, $v_{2T} = 4$ mV, $\tau_e = 4$ ms, $\tau_i = 5.5\tau_e$). Here, we see a branch of type II-AA which is telescoped into a II-AB branch. The initialization of the system (blue and red arrows) determines its behavior (low-amplitude vs. high-amplitude limit cycles). See also the legend of Fig. 2. For example, the system stating at the blue arrow will jump into a state where it produces high-amplitude oscillations after a transient increase in the mean input to the PCs (e.g., by 8 mV) and will remain in this state even after the input has returned to its original state by undergoing the subcritical Andronov–Hopf bifurcation. To return, the system must pass the global (saddle–node) bifurcations by transient decreasing extrinsic input (e.g., by −3 mV).

level, the system returns to its original idle mode by passing a supercritical AH bifurcation (to phase portrait IV). Hence, in contrast to the configuration shown in Fig. 10, the effects of strong input perturbations are reversible by traversing several different states (represented by their respective phase portraits, see Fig. 3).

The third example in Fig. 12 ($v_{1T} = -4$ mV, $v_{2T} = -v_{1T}$, $\tau_e = 14$ ms, $\tau_i = 18$ ms) shows that several branches might coexist separately along the fixed point curve, lined up like beads on a string. This configuration (type II-AA-AA-AA, which makes up about 0.6% of all multibranch configurations) does not result in any sudden changes, but, depending on varying extrinsic input on PCs, the system will alternate between idle or excitation mode, producing harmonic oscillations of different frequencies. If the input to the PCs is noise of sufficiently high amplitude, the output will be a mixture of unfiltered noise and various frequencies generated by the different LCs. This may be the basis for a model of M/EEG spectra featuring several distinct frequency peaks, for example, in the theta and alpha ranges as in this case. Finally, as a fourth example, the standard configuration of Jansen and Rit itself (Fig. 2) demonstrates the coexistence of two branches of LCs of type I-B and II-AA, giving rise to spike-like and sinusoidal activity, respectively. This configuration allows, by virtue of changing the input to the PCs, an abrupt transition from the I-B-cycle (anharmonic oscillations) to the II-AA-cycle (harmonic oscillations), but not vice versa. In Fig. 13, we show how the gradual addition of extrinsic inputs to the IIN changes the bifurcation diagram and causes the system to go through different distinct oscillatory regimes. We assume that the system is exposed to Gaussian input to the PCs (expectation value $E[v_{3T}] = 6.5$ mV and standard deviation $D[v_{3T}] = 1.3$ mV) and there is no extrinsic input to the EINs in this example. With no input to the IINs, this configuration is identical to that of Jansen and Rit and produces waxing and waning harmonic oscillations in the alpha range. If the input to the IIN is increased, the system's behavior, and thus the bifurcation diagram, changes and the system starts to produce large amplitude spike-like anharmonic oscillations of varying frequency. A further increase in the IIN's input moves the system into a state where it generates constant output with overlaid noise (Fig. 13). This demonstrates that the system behavior changes not only along with bifurcations due to the extrinsic inputs on PCs but also along with the bifurcations due to the other codimensions (i.e., extrinsic inputs on both INs). Although we did not analyze codimension five bifurcations, the diagrams in Figs. 5 to 8 give an insight into the system's behavior for the whole parameter space (based on our classification scheme).

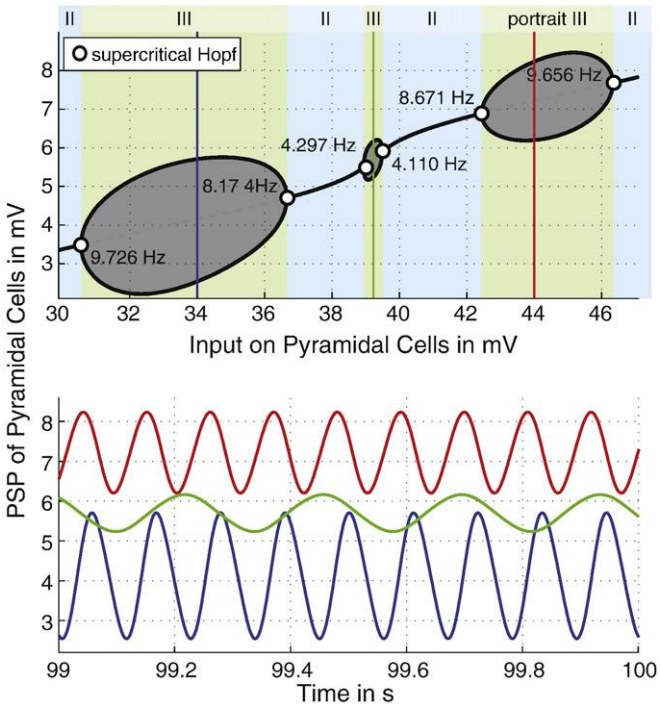

Fig. 12. Sequential existence of several stable limit cycles for different ranges of extrinsic input on pyramidal cells (parameter configuration: $v_{1T} = -4$ mV, $v_{2T} = -v_{1T}$, $\tau_e = 14$ ms, $\tau_i = 18$ ms). The blue, green and red curves indicate the time series for different levels of input to the pyramidal cells. See also the legend of Fig. 2.

Discussion

In this study, we presented a detailed analysis of the dynamic properties of an NMM for a single cortical area. The model is based on the well-known proposal of Jansen and Rit (1995) and was extended by incorporating extrinsic inputs (from other cortical and subcortical areas) on the interneuron populations. We systematically investigated the system's behavior by means of bifurcation diagrams, as a function of its key parameters, which are the extrinsic input levels to all three NMs and the dendritic time constants for excitatory as well as inhibitory synaptic contacts. We determined finite effective ranges for these parameters (Table 1). We argue that variations of the extrinsic input levels are equivalent to variations of the firing thresholds of the NMs and, under certain conditions (see section Dimension reduction), to variations of the intrinsic connection strengths between the NMs, and that therefore our analysis also accounts for the influences of these parameters. Consequently, our analysis can be considered complete.

One aim of the paper was to describe the rich dynamics observed in a systematic way. At the lowest level, we were able to distinguish three principal types of steady state behavior with respect to the PC's postsynaptic potentials. First, stable foci and nodes produce constant output, which, under small perturbation (e.g., noisy input to the PCs), changes into filtered noise with (for foci) or without oscillatory components. Second, supercritical AH bifurcations give rise to stable LCs. They appear gradually upon passage of the bifurcation. Their frequency is relatively insensitive with respect to the level of extrinsic input, and ranges between 0 and 80 Hz, depending on the dendritic time constants (see Fig. 9). For noisy input, this results in waxing and waning harmonic oscillations of relatively stable frequency. This pattern is compatible with typical brain rhythms, such as the alpha rhythm or sleep spindles. Third, global bifurcations, for example of Shil'nikov type, give rise to homoclinic LCs appearing suddenly at high amplitude and low frequency. They are generally not harmonic but have a spike-like appearance (anharmonic oscillation). Their frequency depends a great deal on the input levels. Hence, if the PCs receive fluctuating input, the intervals between the wave peaks (or spikes) are variable. These phenomena are compatible with the hallmark of epileptic seizures (i.e., suddenly occurring, irregular spiking patterns (see, e.g., Marten et al., 2009; Rodrigues et al., 2009; Suffczynski et al., 2005; Wendling et al., 2002; Wendling et al., 2000)). Note that Shil'nikov's bifurcations were also related to "spike-wave" behavior in more theoretical models on M/EEG (e.g., van Veen and Liley, 2006). This relationship was also identified when analyzing M/EEG by using embedding methods (e.g., Friedrich and Uhl, 1996).

The occurrence of and the transitions between these states, as a function of extrinsic inputs, are encoded by the topology of the bifurcation diagrams. This means one can read these transitions directly from the bifurcation diagrams. In general, we found a number of potentially neurobiologically interesting branches of LCs, which allow for sudden entering into orbits or smooth transitions between different LC-regimes by small variations of extrinsic inputs (Fig. 2 and Figs. 10 to 13). These effects were either reversible or irreversible, depending on the parameters and initial state of the system. When moving through the effective parameter space, we observed both

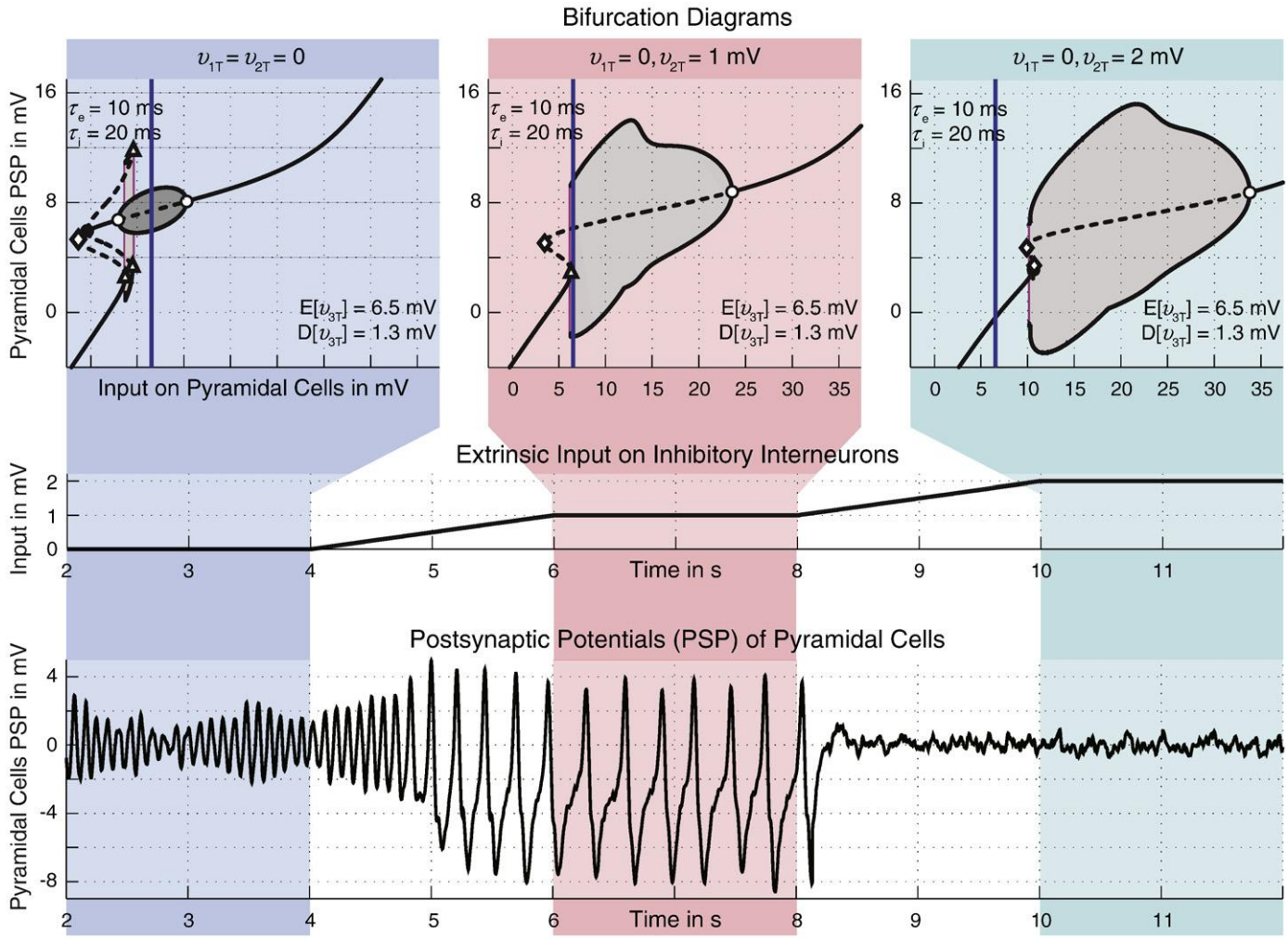

Fig. 13. Extrinsic inputs on inhibitory interneurons change the system behavior. By exciting inhibitory interneurons, the system switches from producing waxing and waning alpha activity in the first state to epileptic spiking-like activity in the second state, and to noise-driven activity in the last state of excitation. The first extrinsic input state on inhibitory interneurons, highlighted in blue, corresponds to Jansen's parameter configuration (i.e., only extrinsic input on pyramidal cells). For the second input state, highlighted in red, the input on inhibitory interneurons is constantly 1 mV and doubles for the third input state. The extrinsic input on the pyramidal cells is Gaussian (with an expectation value of $E[\upsilon_{3T}] = 6.5$ mV and a standard deviation of $D[\upsilon_{3T}] = 1.3$ mV) and zero for the excitatory interneurons during all states. For each state, the bifurcation diagram (of the postsynaptic potential against the extrinsic input on pyramidal cells) is shown in the top row. The input on inhibitory interneurons and the postsynaptic potentials of the pyramidal cells is shown in the middle and bottom rows. Regarding the bifurcation diagrams, circles are sub- (black) and supercritical (white) Andronov–Hopf bifurcations, diamonds are saddle–saddle and triangles are saddle-node bifurcations. The red lines represent global bifurcations (saddle–node like bifurcations in Poincaré maps). The black framed gray areas are the branches of limit cycles. Using the classification of limit cycle branches (see Fig. 4), we identify the first input state as a combination of type I-B and II-AA, the second and third input state of type I-A. The blue lines indicate the expectation value of the Gaussian input on the pyramidal cells. Thus, the alpha activity is caused by harmonic cycles due to Andronov–Hopf bifurcations in the first state and the epileptic spiking-like activity of the second state is caused by homoclinic cycles due to a saddle–node Shil'nikov bifurcation. In the last state, the system is out of reach of any limit cycle and attracted to the equilibrium disturbed by the extrinsic Gaussian input on pyramidal cells.

quantitative changes in the precise location of the bifurcations and LCs and qualitative changes of the entire topology of the bifurcation diagram (e.g., bifurcations appearing or disappearing). Consequently, at another level of description, we introduced a classification of the observed principal types of system topology made up of globally stable LC branches (Fig. 1). By using this classification scheme, we were able to reduce the complexity of the dynamic behavior to a few basic phenomena which exist in isolation or in combination. This enabled us to map these topologies to the parameter space and draw a number of global conclusions about the frequency of occurrence and existence conditions of these topologies (Figs. 5 and 6) and the associated oscillatory regimes (Figs. 7 and 8).

Our systematic analysis revealed that the dynamic behavior (I-B and II-AA topology) of the specific parameter configuration proposed by Jansen and Rit (1995), as reported by the analysis of Grimbert and Faugeras (2006), is an exception rather than the rule with respect to the effective parameter space of the extended model (see Figs. 5 and 6). Hence, the general validity of any analysis based on that configuration depends on the assumption that the parameter set put forward by Jansen and Rit (1995) is adequate within quite narrow bounds (see Figs. 5 and 6, branch type AA-B). Furthermore, we found a bifurcation which was not reported by Grimbert and Faugeras (2006).

There were several general findings concerning the dynamics of the system. First, we showed that harmonic oscillations arising from two AH bifurcations (II-AA type) are by far the most common oscillatory behavior over the entire parameter space (Figs. 5, 6, and 9). This finding is compatible with the widespread presence of relatively frequency-stable rhythms in brain signals (delta, alpha, beta, and gamma frequency band). Anharmonic oscillatory regimes (e.g., in branch type I-B and II-BB, see Fig. 3 for classification or the examples in Fig. 2 and Figs. 10 to 12) are thus special and exceptional, but nonetheless very interesting cases for modeling pathological states (e.g., epilepsy, Figs. 5 to 8).

Second, the analysis revealed that the ratio between the inhibitory and excitatory dendritic time constants (not their absolute values) determines whether no oscillations, only one type of oscillations (harmonic or anharmonic) or both types are possible (Fig. 5) (this confirms the findings of David and Friston, 2003). Regarding the system Eqs. (5) to (11), it is obvious that the dendritic time constants are related to each other by their scaling ratio τ_i/τ_e (e.g., by substituting the dimensionless variable t/τ_e for time variable t). Hence, the system behavior qualitatively depends only on the scaling ratio and on the extrinsic inputs on both INs. More specifically, our analysis revealed that for maintaining an oscillatory regime, it is essential to keep the ratio $\tau_i/\tau_e>0.2$ (Fig. 7).

Third, our analysis showed that the system is more sensitive to extrinsic inputs to IINs than to extrinsic inputs to EINs. Since oscillations in local neuronal circuits depend fundamentally on effective inhibitory feedback loops, extrinsically inhibited IINs prevent the system from oscillating, while moderate extrinsic excitation of IINs causes local neuronal circuits to oscillate. Extrinsic inputs to EINs predominantly influence the spiking behavior of the system (Fig. 8).

Another aim of this study was to demonstrate that it is possible to describe ordered sequences of qualitatively different oscillatory regimes by NMMs, using bifurcation diagrams. Generally, such sequences arise when traversing the parameter space slowly, as compared to the time constants of the oscillations involved. Such slow parameter changes could be associated with numerous neurobiological phenomena, such as changes in attention and vigilance, progression of disease, effects of medication, or changes in sleep stage.

For example, the rapid transition between non-REM and REM sleep accompanied by both drastic changes in rhythmic EEG patterns and numerous functional phenomena has been modeled as phase transition of a NMM very similar to ours, caused by slow parametric changes due to biochemical processes (i.e., changing acetylcholine and adenosine levels) (Steyn-Ross et al., 2005). Another prominent example, where modelers have exploited slow transitions across a bifurcation, is an epileptic seizure, which is characterized by the transition from normal EEG dominated by harmonic alpha or beta oscillations to high-amplitude irregular spike or spike-wave oscillations (Marten et al., 2009; Rodrigues et al., 2009; Suffczynski et al., 2005; Wendling et al., 2002). A further example is the EEG observed over the motor cortex during brisk finger movements, where the brain dynamics change from dominant alpha to increased gamma oscillations during the preparation phase and then to increased beta oscillations shortly after the movement itself. Finally, after a few seconds, the system relapses into its normal state (Pfurtscheller and Lopes da Silva, 1999).

The topologies of LC branches in bifurcation diagrams may be used to describe the formation of such sequences. For instance, Fig. 13 (see Results for a detailed description) shows how a gradual increase in extrinsic inhibition by means of excitatory input to the IINs can suddenly move the system from normal M/EEG featuring alpha waves to high-amplitude irregular spiking.

We also found a number of topologies where the system is constrained to undergo a specific ordered sequence of dynamic states for recovering its initial state after having been perturbed by a transient change of a system parameter. For instance, in Fig. 11, the system first jumps to a state where it produces anharmonic oscillations after a transient increase in the extrinsic input to the PCs. Interestingly, the system will remain in this state even after the input has returned to its original level. The system will only return to its initial state when a transient decrease of sufficient amplitude occurs in the extrinsic input to the PCs. This could be a model, for example, for the elicitation of epileptic seizures by sudden, unexpected stimuli (startle epilepsy). In other configurations, a return to the initial state is impossible (irreversible processes). For instance, Fig. 10 shows the topology of encapsulated II-AA branches of opposite stability. When the normal state (inside the unstable AH–LCs) is perturbed slightly (i.e., below threshold), the system produces damped oscillations, but after passing the threshold (i.e., the unstable AH–LCs), the system is unable to return to its initial state.

These examples (see Results for further details) demonstrate that a multitude of biologically interesting dynamic phenomena in brain signals can be modeled by a rather simple NMM of a single cortical area in conjunction with appropriate input trajectories. Thus, our systematic analysis details the parameter configurations and input trajectories that can be used to model specific changes between different dynamic states.

As we have argued, bifurcations can be a useful tool for modeling M/EEG data. However, they can also be a nuisance when one aims to model a single dynamic regime. For example, if one wants to model stable oscillations, the parameterization should be placed distant from a bifurcation to avoid a transition under slightly varied parameters. The identification of *safe* placements in parameter space is another use of our bifurcation analysis. As we have shown, some dynamic regimes exist, which seem to be quite narrow islands in parameter space (see, e.g., Fig. 5 for branch type combinations: e.g., AA-AB which is restricted to narrow bands of dendritic time constant ratios of either about 1.29 to 1.31 (corresponding to the example in Fig. 10) or about 5.45 to 6.17 (corresponding to the example in Fig. 11)). Such configurations in the parameter space may be exploited for transitions between dynamic regimes but should, in contrast, be avoided for modeling dynamics which are meant to be robust to slight variations in their parameters.

In our analysis, we solely dealt with a local model for a single cortical area. The question arises, whether and under what conditions our results can be generalized to the case of several interacting local neuronal circuits. Our results directly predict the behavior of networks consisting of local units under the assumption of weak and/or slowly varying extrinsic inputs (relative to the dendritic time constants of the local neuronal circuit). If this is not the case, for example, if several cortical areas have relatively strong bidirectional coupling, more complex state spaces would have to be explored. However, given the effective ranges of the extrinsic inputs to a single cortical area, one can also determine the ranges for the connection strengths between areas. This means that the local neuronal circuits greatly limit the behavior of the entire network. To keep a large network in an operating state, connections between interacting brain areas must not exceed these effective ranges. This implies the presence of regulatory mechanisms, for example, neurotransmitter receptor adoption (Moran et al., 2007; Wright et al., 2003), synaptic plasticity (David and Friston, 2003; Moran et al., 2007; Wright et al., 2003), or back-propagating action potentials into the dendritic tree (Wright et al., 2003).

Our results enable the efficient definition of prior distributions of parameters in Bayesian model inversion, as used in DCM (David et al., 2006; Kiebel et al., 2009b). To model specific phenomena using DCM, the researcher would first select specific regimes of parameters, informed by the present bifurcation analysis. By using appropriate prior distribution centered on the selected parameter configuration, the researcher can then constrain the effective ranges for the extrinsic input levels and inter-area connection strengths. Additionally, the initial value problem of the gradient-ascent estimation scheme used by DCM can be addressed by informing the inversion scheme about qualitatively different dynamic regimes. In principle, this would enable DCM users to more effectively identify global maxima of the objective function by starting the inversion process repeatedly in qualitatively different dynamic regimes.

NMM dynamics account for coherent activity of large numbers of neurons, which is exactly the kind of phenomena that give rise to EEG and MEG. These signals are known to reflect important aspects of brain function. In particular, it has been shown that oscillatory activity observed using M/EEG bears a strong relationship with brain function in both health and disease. Widespread brain oscillations reflect the

cortical arousal state, as they seem to be associated with the α-rhythm (8–12 Hz) in the visual cortex (see, e.g., Klimesch, 1999), the μ-rhythm (~10 Hz and ~20 Hz) in the somatomotor cortex (Pfurtscheller, 1989; Salmelin et al., 1995; Salmelin and Hari, 1994), and the τ-rhythm (8–12 Hz) in the auditory cortex (Hari and Salmelin, 1997). Such rhythms are selectively suppressed by primary sensory or motor activity (Pfurtscheller and Lopes da Silva, 1999). Other brain rhythms are directly related to active processes. For example, frontal β-rhythms (~20 Hz) are associated with motor activity (Hari and Salmelin, 1997; Pfurtscheller and Lopes da Silva, 1999; Spiegler et al., 2004), hippocampal θ-rhythms (4–8 Hz) as well as γ-rhythms (30–80 Hz) in various brain parts play an important role for memory function (Burgess and Ali, 2002; Burgess and Gruzelier, 1997; Herrmann et al., 2004; Kahana et al., 1999; Klimesch, 1996, 1999; Klimesch et al., 1996, 1997; Lisman and Idiart, 1995; Llinás and Ribary, 1993), and γ-rhythms appear to reflect processes of perceptual binding in the visual (Gray and Singer, 1989; Herrmann and Mecklinger, 2000; Tallon-Baudry et al., 1997; Tallon-Baudry et al., 1996) and auditory domains (Knief et al., 2000; Pantev et al., 1993, 1991). Pathological brain function is strongly correlated with typical brain oscillations, for example in epilepsy during seizures (Destexhe and Sejnowski, 2001) and in Parkinson's disease (Gross et al., 2001; Schnitzler and Gross, 2005; Tass et al., 1998). This relevance of oscillatory M/EEG phenomena for brain function corroborates the view that modeling neural mass action is important for the understanding of brain function and the organization of behavior (Deco et al., 2008; Freeman, 1975, 2002). It is worth mentioning that with realistic choices of the system parameters, the neural mass model (Eqs. (5) to (11)) generates a range of frequencies covering most of the reported functionally relevant M/EEG rhythms.

Moreover, as discussed above, many functional processes in the brain can be described as a succession of distinct functional states, mirrored by specific oscillatory regimes observed in experimental M/EEG data. Often, this succession of states seems to be caused by a gradual evolution of certain system parameters. For example, during sleep, slowly decreasing levels of adenosine and other somnogens cause a steady downward shift in resting potential (equivalent to shift in extrinsic input level, see section Parameter space), while acetylcholine levels, raising the excitability of excitatory neurons and decreasing the gain of excitatory synapses, perform slow (~90 minutes) cycles. These slow biochemical trajectories are believed to be responsible for the repetitive transition between slow wave and REM sleep phases (Hasselmo, 1995; Steyn-Ross et al., 2005). We have shown that bifurcation analysis provides a generative model for exactly this type of phenomenon: a gradually changing system parameters lead to a sequence of distinct dynamic regimes with relatively rapid transitions between them.

In conclusion, we present the first complete account of the dynamic behavior of an NMM of a cortical area, of which, so far, only one special parameter configuration had been investigated (Grimbert and Faugeras, 2006). We systematically describe the dynamic richness of the system using a relatively small set of prototypical system topologies. This enabled us to draw general conclusions about the interesting phenomena and their conditions of existence. Moreover, we identified biologically relevant configurations and showed how reversible and irreversible transitions between different oscillatory regimes, which can be observed in M/EEG, can be explained by smooth changes in the extrinsic inputs. In this way, we obtain generative models for ordered sequences of dynamic phenomena, which may be used as models of sudden transitions between qualitatively brain states, caused by slow changes in system parameters.

Acknowledgments

This work was supported by the Max Planck Society and the Deutsche Forschungs-gemeinschaft (grant KN588/3).

References

Abbott, L.F., 1999. Lapique's introduction of the integrate-and-fire model neuron (1907). Brain Res. Bull. 50, 303–330.
Agmon-Snir, H., Segev, I., 1993. Signal delay and input synchronization in passive dendritic structures. J. Neurophysiol. 70, 2066–2085.
Ahmed, B., Anderson, J.C., Martin, K.A., Nelson, J.C., 1997. Map of the synapses onto layer 4 basket cells of the primary visual cortex of the cat. J. Comp. Neurol. 380, 230–242.
Attwell, D., Laughlin, S.B., 2001. An energy budget for signaling in the grey matter of the brain. J. Cereb. Blood Flow Metab. 21, 1133–1145.
Braitenberg, V., Schüz, A., 1991. Anatomy of the Cortex : Statistics and Geometry. Springer-Verlag, Berlin; New York.
Breakspear, M., Jirsa, V.K., 2007. Neuronal dynamics and brain connectivity. In: Jirsa, V.K., McIntosh, A.R. (Eds.), Handbook of Brain Connectivity. Springer, Berlin, Heidelberg, pp. 3–64.
Burgess, A., Ali, L., 2002. Functional connectivity of gamma EEG activity is modulated at low frequency during conscious recollection. Int. J. Psychophysiol. 46, 91–100.
Burgess, A.P., Gruzelier, J.H., 1997. Short duration synchronization of human theta rhythm during recognition memory. NeuroReport 8, 1039–1042.
David, O., Friston, K.J., 2003. A neural mass model for MEG/EEG: coupling and neuronal dynamics. NeuroImage 20, 1743–1755.
David, O., Harrison, L., Friston, K.J., 2005. Modelling event-related responses in the brain. NeuroImage 25, 756–770.
David, O., Kiebel, S.J., Harrison, L.M., Mattout, J., Kilner, J.M., Friston, K.J., 2006. Dynamic causal modeling of evoked responses in EEG and MEG. NeuroImage 30, 1255–1272.
Deco, G., Jirsa, V.K., Robinson, P.A., Breakspear, M., Friston, K., 2008. The dynamic brain: from spiking neurons to neural masses and cortical fields. PloS Computat. Biol. 4.
Destexhe, A., Sejnowski, T.J., 2001. Thalamocortical Assemblies: How Ion Channels, Single Neurons and Large-scale Networks Organize Sleep Oscillations1st ed. Oxford University Press, Oxford.
Ermentrout, B., 1998. Neural networks as spatio-temporal pattern-forming systems. Rep. Prog. Phys. 61, 353–430.
Felleman, D.J., Van Essen, D.C., 1991. Distributed hierarchical processing in the primate cerebral cortex. Cereb. Cortex 1, 1–47.
FitzHugh, R., 1955. Mathematical models of threshold phenomena in the nerve membrane. Bull. Math. Biophys. 17, 257–278.
Freeman, W.J., 1975. Mass Action in the Nervous System: Examination of the Neurophysiological Basis of Adaptive Behavior through the EEG. Academic Press, New York.
Freeman, W.J., 1978. Models of the dynamics of neural populations. Electroencephalogr. Clin. Neurophysiol. [suppl] 34, 9–18.
Freeman, W.J., 2002. Neurodynamics: An Exploration in Mesoscopic Brain Dynamics1st ed. Springer, London.
Friedrich, R., Uhl, C., 1996. Spatio-temporal analysis of human electroencephalograms: Petit-mal epilepsy. Phys. D 98, 171–182.
Friston, K.J., T., A.J., Kiebel, S.J., Nichols, T.E., Penny, W.D., 2007. Statistical Parametric Mapping: The Analysis of Functional Brain Images 1st ed. Elsevier/Academic Press, Amsterdam ; Boston.
Garrido, M.I., Kilner, J.M., Kiebel, S.J., Friston, K.J., 2007. Evoked brain responses are generated by feedback loops. Proc. Natl. Acad. Sci. U. S. A. 104, 20961–20966.
Garrido, M.I., Kilner, J.M., Kiebel, S.J., Friston, K.J., 2009. Dynamic causal modeling of the response to frequency deviants. J. Neurophysiol. 101, 2620–2631.
Gerstner, W., Kistler, W.M., 2002. Spiking Neuron Models: Single Neurons, Populations, Plasticity. Cambridge University Press, Cambridge, U.K. ; New York.
Glendinning, P., Sparrow, C., 1996. Shilnikov's saddle–node bifurcation. Int. J. Bifurc. Chaos 6, 1153–1160.
Gray, C., Singer, W., 1989. Stimulus-specific neuronal oscillations in orientation columns of cat visual cortex. Proc. Natl. Acad. Sci. U. S. A. 86, 1698–1702.
Grimbert, F., Faugeras, O., 2006. Bifurcation analysis of Jansen's neural mass model. Neural Comput. 18, 3052–3068.
Gross, J., Kujala, J., Hamalainen, M., Timmermann, L., Schnitzler, A., Salmelin, R., 2001. Dynamic imaging of coherent sources: studying neural interactions in the human brain. Proc. Natl. Acad. Sci. U. S. A. 98, 694–699.
Gulledge, A.T., Kampa, B.M., Stuart, G.J., 2005. Synaptic integration in dendritic trees. J. Neurobiol. 64, 75–90.
Hari, R., Salmelin, R., 1997. Human cortical oscillations: a neuromagnetic view through the skull Trends Neurosci. 20, 44–49.
Hasselmo, M.E., 1995. Neuromodulation and cortical function: modeling the physiological basis of behavior. Behav. Brain Res. 67, 1–27.
Herrmann, C., Mecklinger, A., 2000. Magnetoencephalographic responses to illusory figures: early evoked gamma is affected by processing of stimulus features. Int. J. Psychophysiol. 38, 265–281.
Herrmann, C., Munk, M., Engel, A., 2004. Cognitive functions of gamma-band activity: memory match and utilization. Trends Cogn. Sci. 8, 347–355.
Hindmarsh, J.L., Rose, R.M., 1984. A model of neuronal bursting using three coupled first order differential equations. Proc. R. Soc. Lond., Ser. B 221, 87–102.
Hodgkin, A.L., Huxley, A.F., 1952. A quantitative description of membrane current and its application to conduction and excitation in nerve. J. Physiol. 117, 500–544.
Horton, J.C., Adams, D.L., 2005. The cortical column: a structure without a function. Philos. Trans. R. Soc. B Biol. Sci. 360, 837–862.
Jack, J.J.B., Noble, D., Tsien, R., 1975. Electric Current Flow in Excitable Cells. Clarendon Press, Oxford.
Jansen, B.H., Rit, V.G., 1995. Electroencephalogram and visual evoked potential generation in a mathematical model of coupled columns. Biol. Cybern. 73, 357–366.
Jansen, B.H., Zouridakis, G., Brandt, M.E., 1993. A neurophysiologically-based mathematical model of flash visual evoked potentials. Biol. Cybern. 68, 275–283.

Jirsa, V.K., Haken, H., 1996. Field theory of electromagnetic brain activity. Phys. Rev. Lett. 77, 960–963.
Kahana, M., Sekuler, R., Caplan, J., Kirschen, M., Madsen, J., 1999. Human theta oscillations exhibit task dependence during virtual maze navigation. Nature 399, 781–784.
Kiebel, S.J., David, O., Friston, K.J., 2006. Dynamic causal modelling of evoked responses in EEG/MEG with lead field parameterization. NeuroImage 30, 1273–1284.
Kiebel, S.J., Garrido, M.I., Friston, K.J., 2007. Dynamic causal modelling of evoked responses: the role of intrinsic connections. NeuroImage 36, 332–345.
Kiebel, S.J., Garrido, M.I., Moran, R., Chen, C.C., Friston, K.J., 2009a. Dynamic causal modeling for EEG and MEG. Hum. Brain. Mapp. 30, 1866–1876.
Kiebel, S.J., Garrido, M.I., Moran, R., Chen, C.C., Friston, K.J., 2009b. Dynamic causal modeling for EEG and MEG. Hum. Brain Mapp. 30, 1866–1876.
Klimesch, W., 1996. Memory processes, brain oscillations and EEG synchronization. Int. J. Psychophysiol. 24.
Klimesch, W., 1999. EEG alpha and theta oscillations reflect cognitive and memory performance: a review and analysis. Brain Res. Rev. 29, 169–195.
Klimesch, W., Doppelmayr, M., Russegger, H., Pachinger, T., 1996. Theta band power in the human scalp EEG and the encoding of new information. NeuroReport 7, 1235–1240.
Klimesch, W., Doppelmayr, M., Schimke, H., Ripper, B., 1997. Theta synchronization in a memory task. Psychophysiology 34, 169–176.
Knief, A., Schulte, M., Bertran, O., Pantev, C., 2000. The perception of coherent and non-coherent auditory objects: a signature in gamma frequency band. Hear. Res. 145, 161–168.
Kuznetsov, Y.A., 1998. Elements of Applied Bifurcation Theory2 ed. Springer, Berlin.
Liley, D.T.J., Cadusch, P.J., Dafilis, M.P., 2002. A spatially continuous mean field theory of electrocortical activity. Netw. Comput. Neural Syst. 13, 67–113.
Lisman, J., Idiart, M., 1995. Storage of 7+/−2 short-term memories in oscillatory subcycles. Science 267, 1512–1515.
Llinás, R., Ribary, U., 1993. Coherent 40-Hz oscillation characterizes dream state in human. Proc. Natl. Acad. Sci. U. S. A. 90, 2078–2081.
Lopes da Silva, F., van Rotterdam, A., 1999a. Biophysical aspects of EEG and magnetoencephalogram generation. In: Niedermeyer, E., Lopes da Silva, F. (Eds.), Electroencephalography. Clinical Applications, and Related Fields. Williams & Wilkins, Baltimore, Basic Principles, pp. 93–109.
Lopes da Silva, F., van Rotterdam, A., 1999b. Biophysical aspects of EEG and Magnetoencephalogram generation. In: Niedermeyer, E., Lopes da Silva, F. (Eds.), Electroencephalography. Clinical Applications and Related Fields. Williams & Wilkins, Baltimore, Basic Principles, pp. 93–109.
Lopes da Silva, F.H., Hoeks, A., Smits, H., Zetterberg, L.H., 1974. Model of brain rhythmic activity. The alpha-rhythm of the thalamus. Kybernetik 15, 27–37.
Lopes da Silva, F.H., Van Rotterdam, A., Barts, P., Van Heusden, E., Burr, W., 1976. Models of neuronal populations the basic mechanisms of rhythmicity. In: Corner, M.a., Swaab, D.F. (Eds.), Progress in Brain Research, Vol. 45. Perspectives in Brain Research. 9th International Summer School. Amsterdam, Netherlands, July 28–Aug. 1. 1975. Xii + 489p. Illus. Elsevier Scientific Publishing Company, Amsterdam, Netherlands. (Dist. in USA and Canada by Elsevier-North-Holland, Inc., New York, N.Y.), pp. 281–308. ISBN 0-444-41457-6.
Markram, H., Toledo-Rodriguez, M., Wang, Y., Gupta, A., Silberberg, G., Wu, C., 2004. Interneurons of the neocortical inhibitory system. Nat. Rev. Neurosci. 5, 793–807.
Marreiros, A.C., Daunizeau, J., Kiebel, S.J., Friston, K.J., 2008. Population dynamics: variance and the sigmoid activation function. NeuroImage 42, 147–157.
Marten, F., Rodrigues, S., Benjamin, O., Richardson, M.P., Terry, J.R., 2009. Onset of polyspike complexes in a mean-field model of human electroencephalography and its application to absence epilepsy. Philos. Trans. R. Soc. Math. Phys. Eng. Sci. 367, 1145–1161.
Moran, R.J., Kiebel, S.J., Stephan, K.E., Reilly, R.B., Daunizeau, J., Friston, K.J., 2007. A neural mass model of spectral responses in electrophysiology. NeuroImage 37, 706–720.
Moran, R.J., Stephan, K.E., Seidenbecher, T., Pape, H.C., Dolan, R.J., Friston, K.J., 2009. Dynamic causal models of steady-state responses. NeuroImage 44, 796–811.
Mountcastle, V.B., 1957. Modality and topographic properties of single neurons of cats somatic sensory cortex. J. Neurophysiol. 20, 408–434.
Nagumo, J., Arimoto, S., Yoshizawa, S., 1962. An active pulse transmission line simulating nerve axon. Proc. IRE 50, 2061–2070.
Nawrot, M.P., Boucsein, C., Rodriguez-Molina, V., Aertsen, A., Grun, S., Rotter, S., 2007. Serial interval statistics of spontaneous activity in cortical neurons in vivo and in vitro. Neurocomputing 70, 1717–1722.
Nelder, J.A., Mead, R., 1965. A simplex method for function minimization. Comput. J. 7, 308–313.
Nunez, P., 1974. The brain wave equation: a model for the EEG. Math. Biosci. 21, 279–297.
Pantev, C., Elbert, T., Makeig, S., Hampson, S., Eulitz, C., Hoke, M., 1993. Relationship of transient and steady-state auditory evoked fields. Electroenceph. Clin. Neurophysiol. 88, 389–396.
Pantev, C., Makeig, S., Hoke, M., Galambos, R., Hampson, S., Gallen, C., 1991. Human auditory evoked gamma-band magnetic fields. Proc. Natl. Acad. Sci. U. S. A. 88, 8996–9000.
Perko, L., 2001. Differential Equations and Dynamical Systems3rd ed. Springer, New York.
Pfurtscheller, G., 1989. Functional topography during sensorymotor activation studied with event-related desynchronization mapping J. Clin. Neurophysiol. 6, 75–84.
Pfurtscheller, G., Lopes da Silva, F.H., 1999. Event-related EEG/MEG synchronization and desynchronization: basic principles. Clin. Neurophysiol. 110, 1842–1857.
Rall, W., 1964. Theoretical significance of dendritic trees for neuronal input–output relations. In: Reiss, R.F. (Ed.), In Neural Theory and Modeling. Stanford Univ. Press.
Rall, W., 1967. Distinguishing theoretical synaptic potentials computed for different soma-dendritic distributions of synaptic input. J. Neurophysiol. 30, 1138–1168.
Robinson, P.A., Rennie, C.J., Rowe, D.L., 2002. Dynamics of large-scale brain activity in normal arousal states and epileptic seizures. Phys. Rev. E 65.
Rodrigues, S., Barton, D., Szalai, R., Benjamin, O., Richardson, M.P., Terry, J.R., 2009. Transitions to spike-wave oscillations and epileptic dynamics in a human cortico-thalamic mean-field model. J. Comput. Neurosci. 27, 507–526.
Salmelin, R., Hari, R., 1994. Spatiotemporal characteristics of sensorimotor neuromagnetic rhythms related to thumb movement. Neurosci. Lett. 60, 537–550.
Salmelin, R., Forss, N., Knuutila, J., Hari, R., 1995. Bilateral activation of the human somatomotor cortex by distal hand movements. Electroenceph. Clin. Neurophysiol. 95, 444–452.
Schnitzler, A., Gross, J., 2005. Normal and pathological oscillatory communication in the brain. Nat. Rev. Neurosci. 6, 285–296.
Schofield, T.M., Iverson, P., Kiebel, S.J., Stephan, K.E., Kilner, J.M., Friston, K.J., Crinion, J.T., Price, C.J., Leff, A.P., 2009. Changing meaning causes coupling changes within higher levels of the cortical hierarchy. Proc. Natl. Acad. Sci. U. S. A. 106, 11765–11770.
Shenoy, K.V., Churchland, M.M., Santhanam, G., Yu, B.M., Ryu, S.I., 2003. Influence of Movement Speed on Plan Activity in Monkey Pre-motor Cortex and Implications for High-Performance Neural Prosthetic System Design. EEE EMBS 25th Annual Meeting. Cancun, Mexico, pp. 1897–1900.
Shil'nikov, L.P., 1969. On a new type of bifurcation of multidimensional dynamic systems. Dokl. Akad. Nauk SSSR 189, 59–&.
Sotero, R.C., Trujillo-Barreto, N.J., Iturria-Medina, Y., Carbonell, F., Jimenez, J.C., 2007. Realistically coupled neural mass models can generate EEG rhythms. Neural Comput. 19, 478–512.
Spiegler, A., Graimann, B., Pfurtscheller, G., 2004. Phase coupling between different motor areas during tongue-movement imagery. Neurosci. Lett. 369, 50–54.
Spruston, N., 2008. Pyramidal neurons: dendritic structure and synaptic integration. Nat. Rev. Neurosci. 9, 206–221.
Staiger, J.F., Flagmeyer, I., Schubert, D., Zilles, K., Kotter, R., Luhmann, H.J., 2004. Functional diversity of layer IV spiny neurons in rat somatosensory cortex: quantitative morphology of electrophysiologically characterized and biocytin labeled cells. Cereb. Cortex 14, 690–701.
Steyn-Ross, D.A., Steyn-Ross, M.L., Sleigh, J.W., Wilson, M.T., Gillies, I.P., Wright, J.J., 2005. The sleep cycle modelled as a cortical phase transition. J. Biol. Phys. 31, 547–569.
Stratford, K.J., Tarczy-Hornoch, K., Martin, K.A., Bannister, N.J., Jack, J.J., 1996. Excitatory synaptic inputs to spiny stellate cells in cat visual cortex. Nature 382, 258–261.
Suffczynski, P., Lopes da Silva, F., Parra, J., Velis, D., Kalitzin, S., 2005. Epileptic transitions: model predictions and experimental validation. J. Clin. Neurophysiol. 22, 288–299.
Tallon-Baudry, C., Bertrand, O., Delpuech, C., Pernier, J., 1996. Stimulus specificity of phase-locked and non-phase-locked 40 Hz visual responses in human. J. Neurosci. 16, 4240–4249.
Tallon-Baudry, C., Bertrand, O., Delpuech, C., Permier, J., 1997. Oscillatory gamma-band (30–70 Hz) activity induced by a visual search task in humans. J. Neurosci. 17, 722–734.
Tass, P., Rosenblum, M.G., Weule, J., Kurths, J., Pikovsky, A., Volkmann, J., Schnitzler, A., Freund, H.-J., 1998. Detection of N:M phase locking from noisy data: application to magnetoencephalography. Phys. Rev. Lett. 81, 3291–3294.
Thomson, A.M., Bannister, A.P., 2003. Interlaminar connections in the neocortex. Cereb. Cortex 13, 5–14.
van Veen, L., Liley, D.T., 2006. Chaos via Shilnikov's saddle–node bifurcation in a theory of the electroencephalogram. Phys. Rev. Lett. 97, 208101.
Wendling, F., Bellanger, J.J., Bartolomei, F., Chauvel, P., 2000. Relevance of nonlinear lumped-parameter models in the analysis of depth-EEG epileptic signals. Biol. Cybern. 83, 367–378.
Wendling, F., Bartolomei, F., Bellanger, J.J., Chauvel, P., 2002. Epileptic fast activity can be explained by a model of impaired GABAergic dendritic inhibition. Eur. J. Neurosci. 15, 1499–1508.
Williams, S.R., Stuart, G.J., 2003. Role of dendritic synapse location in the control of action potential output. Trends Neurosci. 26, 147–154.
Wilson, H.R., Cowan, J.D., 1972. Excitatory and inhibitory interactions in localized populations of model neurons. Biophys. J. 12, 1–24.
Wright, J.J., Rennie, C.J., Lees, G.J., Robinson, P.A., Bourke, P.D., Chapman, C.L., Gordon, E., Rowe, D.L., 2003. Simulated electrocortical activity at microscopic, mesoscopic, and global scales. Neuropsychopharmacology 28 (Suppl. 1), S80–S93.